Analyzing Late Harmattan Dust Effects on Subsequent Early Rainfall Around West Africa's Cocoa Belt Using Sentinel-5P TROPOMI Satellite Data

by

Kaori Niki

to obtain the degree of Master of Science
at the Delft University of Technology,
to be defended publicly on Tuesday July 15, 2025 at 1:00 PM.

Student number:	5943965	
Project duration:	February 1, 2025 – July 15, 2025	
Thesis committee:	Prof. dr. ir. N (Nick) van de Giesen,	TU Delft, supervisor
	Prof. dr. ir. HWJ (Herman) Russchenberg,	TU Delft, supervisor
	Dr. JP (Pepjin) Veefkind,	TU Delft, supervisor

TU Delft

Highlights

Analyzing Late Harmattan Dust Effects on Subsequent Early Rainfall Around West Africa's Cocoa Belt Using Sentinel-5P TROPOMI Satellite Data

Kaori Niki

- Strong positive correlations between late Harmattan dust and early rainfall were found in the southwestern Côte d'Ivoire and southern Liberia in the high-cocoa production area, aligning with anecdotal evidence from a local farmer
- This showed a potential of using Harmattan dust in February-March to forecast early rainfall in April-May
- High-resolution Sentinel-5P TROPOMI data allowed detailed analysis of the impacts of Harmattan

Analyzing Late Harmattan Dust Effects on Subsequent Early Rainfall Around West Africa's Cocoa Belt Using Sentinel-5P TROPOMI Satellite Data

Kaori Niki[a,1]

[a]*Delft University of Technology, Delft, The Netherlands*

Abstract

This study analyzed the relationship between late Harmattan dust in February-March and subsequent early rainfall in April-May in West Africa, focusing around the high cocoa-producing regions. The impact of Harmattan was evaluated using high-resolution Sentinel-5P TROPOMI data. Strong positive correlations were found in the southwestern regions of Côte d'Ivoire and southern Liberia where cocoa production is prominent. This is consistent with anecdotal evidence obtained from a local farmer in Gagnoa, which falls under the positively correlated area found in this study. The findings suggest that late Harmattan dust may serve as a potential indicator of early rainfall. This could help better agricultural planning for local farming communities, given the significant influence of rainfall amount on cocoa growth.

Keywords: Harmattan, Aerosol Index, TROPOMI, Sentinel-5P, Cocoa Production, Rainfall, IMERG Harmattan, Aerosol Index, TROPOMI, Sentinel-5P, Cocoa Production, Rainfall, IMERG

1. Introduction

Harmattan is a seasonal north-easterly wind that occurs in West Africa that brings dry and cold air, typically in the late fall and winter from November to March (Sunnu et al., 2008; McTainsh, 1980). This phenomenon is primarily driven by the combinations of subtropical high-pressure systems and the Intertropical Convergence Zone, which influences its onset, duration, and intensity (Schwanghart and Schütt, 2008; Anuforom et al., 2007; Balarabe et al., 2016). Harmattan carries very fine dust from the Sahara desert. Specifically, the Bodélé Depression in the Republic of Chad has been

found to be the main source around Niger and surrounding West African regions (Hamilton et al., 1945; Adetunji and Ong, 1989; Sunnu et al., 2008). However, recent findings suggest that the settled dust may be of local origin in areas lying further south, such as Ghana (Lyngsie et al., 2011).

Although these dusts may locally help improve the structure and nutrient content of the soil, they often have negative influences on the environment and human health. This includes smothering of young plants, causing diseases such as pneumonia, skin irritation; as well as reducing visibility, relative humidity, and temperature (Hayward and Oguntoyinbo, 2019; Chiemeka and Chineke, 2009; McTainsh, 1980; Adetunji and Ong, 1989; Schwanghart and Schütt, 2008). Beyond these localized effects, Harmattan also impacts larger-scale climate systems, such as the radiative balance and microphysical properties of clouds, which subsequently impact weather patterns (Aweda et al., 2023). Despite the wide-ranging impacts, many aspects of Harmattan and its influence remain underexplored.

Recent advances in satellite remote sensing technology have enabled monitoring of the spatio-temporal distribution of dust sources (Schepanski et al., 2017; Tegen et al., 2013). The Ultraviolet Aerosol Index (UVAI), often derived from satellite observations, has been widely used for such analyses. Regarding dust in Africa, the UVAI from the Total Ozone Mapping Spectrometer (TOMS) and the Ozone Monitoring Instrument (OMI) have been used in several studies (Herman et al., 1997; Torres et al., 2007; Balarabe et al., 2015). Furthermore, Harmattan dust and its associated impacts have also been assessed using UVAI, such as investigations into the variability of UV-absorbing aerosols (Anuforom et al., 2007) and long-term trends of Harmattan dust over thirty years (Balarabe, 2019).

In October 2017, the Sentinel 5-Precursor (S5P) satellite was launched carrying the TROPOspheric Monitoring Instrument (TROPOMI) with the aim of monitoring Earth's atmosphere focusing on air quality and climate change (Veefkind et al., 2012). Compared to its predecessors, TROPOMI provides data at significantly higher spatial resolution with a high signal-to-noise ratio, enabling more detailed and precise observations. This helps improve the understanding of atmospheric environments, and in particular, could enable a better analysis of Harmattan events and their impacts through the use of UVAI product. Recent applications of UVAI from S5P/TROPOMI on dust events include the analysis of a dust storm in the Algerian Sahara (Guehaz et al., 2024) and monitoring of dust weather in East Asia (Zhang et al., 2025). These showed the ability to perform a detailed analysis in

specific regions using the high-resolution S5P/TROPOMI data.

This study aims to investigate the local belief in West Africa that the dustier Harmattan causes more rainfall in the subsequent rainy season. This hypothesis is based on anecdotal evidence from a local farmer from West Africa, around Gagnoa in Côte d'Ivoire, but has not been scientifically examined. Understanding this relationship is especially critical in the southern part of West Africa, which lies within the Cocoa Belt, known for its high cocoa production. Over the years, rainfall variability has significantly affected cocoa production: droughts have hindered growth, while excessive rainfall has caused the spread of multiple diseases (Adet et al., 2024; Asitoakor et al., 2022). Cocoa farming is a vital part of the economy in these countries, contributing significantly to their Gross Domestic Product (GDP) as well as providing notable employment (Taylor et al., 2025; Yao et al., 2025). If the Harmattan intensity relationships that serve as an early indicator of the upcoming rainfall season can be clarified, they could serve as a valuable tool for agricultural planning and forecasting.

To address this gap, this study utilizes high-resolution satellite data of the UVAI product from the S5P/TROPOMI to investigate the impact of Harmattan dust on the subsequent rainfall season across southern West Africa's cocoa-producing regions and nearby areas.

2. Study Area

This study focuses on the southern coastal regions around the Cocoa Belt in West Africa: Liberia, Côte d'Ivoire, and Ghana, as shown in Figure 1 (latitude: 4°N to 11°N; longitude: 1.2°E to 11.5°W). Based on 1991–2020 climate averages, annual rainfall totals are approximately 2,450 mm in Liberia, 1,230 mm in Côte d'Ivoire, and 1,210 mm in Ghana. Maximum temperatures during the hottest months (March - May) reach 31.7 °C, 33.8 °C, and 34.7 °C respectively (World Bank, 2025).

Côte d'Ivoire and Ghana are leading producers of cocoa; for instance, in the 2022/23 season, the productions were 2241 and 654 thousand tonnes respectively, together accounting for more than 57 % of the world's cocoa production(International Cocoa Organization, 2025). The orange dashed line area shows the climatically most suitable cocoa production districts in Côte d'Ivoire and Ghana (Läderach et al., 2013). These regions correspond to the cocoa farm locations identified using remote sensing data (Abu et al., 2021). The regions with light blue dots indicate the highest concentrations of cocoa

plantations detected in the same study. While cocoa is grown extensively in the southern regions of Côte d'Ivoire and Ghana, production in Liberia is much lower by comparison and more geographically scattered, though primarily concentrated in Nimba, Lofa, and Bong counties (Schroth et al., 2015). Optimal cocoa-growing conditions include 1,500-2,000 mm of annual rainfall, with dry periods — periods less than 100 mm/month — not exceeding three months (International Cocoa Organization). Additionally, maximum temperatures up to 32 °C are considered ideal for crop development (Climate Central, 2025).

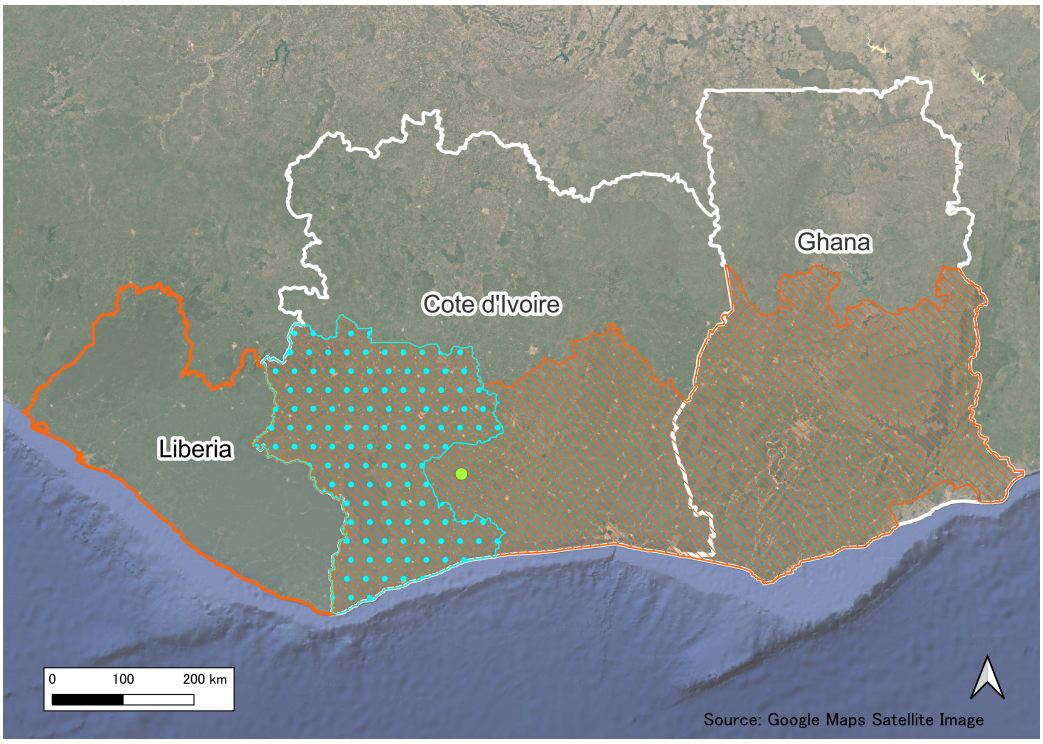

Figure 1: Map of Liberia, Côte d'Ivoire, and Ghana. The orange dashed line area indicates the cocoa production region and light blue dotted area indicates the districts with highest concentration of cocoa production within according to (Abu et al., 2021). In Liberia, cocoa production is scattered across the country. The light green dot represents Gagnoa, the location of the local farmer who provided the anecdotal evidence.

3. Materials and Methodology

3.1. Overview of Methodology

Satellite-derived UVAI and precipitation data were used to examine the impact of Harmattan dust on the subsequent rainfall season. Desert dust was estimated from UVAI values obtained from the S5P/TROPOMI data, with non-dust UV-absorbing aerosols excluded based on established filtering criteria. As part of the filtering process, a threshold based on carbon monoxide (CO) concentrations was applied, which were also obtained from S5P/TROPOMI dataset. Daily precipitation data were obtained from the Integrated Multi-satellitE Retrievals for the Global Precipitation Measurement (GPM) mission (IMERG). Both dust and rainfall data were averaged over selected months corresponding to the Harmattan and rainfall seasons. Because the rainfall data had a coarser spatial resolution, it was refined to match the resolution of the dust data. Correlations between dust and rainfall were then computed for different temporal pairs and statistical significance tests were performed. A schematic overview of the methodology is provided in Figure 2.

Four temporal pairs of Harmattan dust and rainfall periods as shown below were evaluated in this study. For each pair, UVAI and precipitation values were averaged over the entire specified months for each pixel to conduct the correlation analysis:

- Full Harmattan period (November–March) → Full rainfall season (April–September)
- Full Harmattan period (November–March) → Early rainfall season (April–May)
- Late Harmattan period (February–March) → Full rainfall season (April–September)
- Late Harmattan period (February–March) → Early rainfall season (April–May)

For the analysis with an early rainfall season, seven years of data were used, while for the analysis with a full rainfall season, six years of data were used due to the availability of the data for 2025. Due this limitations in the temporal availability, the Global Ozone Monitoring Experiment-2 (GOME-2) Absorbing Aerosol Index (AAI) data and the Measurement of Pollution

in the Troposphere (MOPITT) Carbon Monoxide (CO) data were used to evaluate Harmattan over 2007-2021, along with IMERG Final Run rainfall data. This was conducted to cover a longer time-span. However, the spatial resolution of the dust data obtained using GOME-2 & MOPITT data was much coarser compared to S5P/TROPOMI data, resulting in less detailed observations. The details of the datasets and the analyses are presented outside the main results and are included in Appendix A.

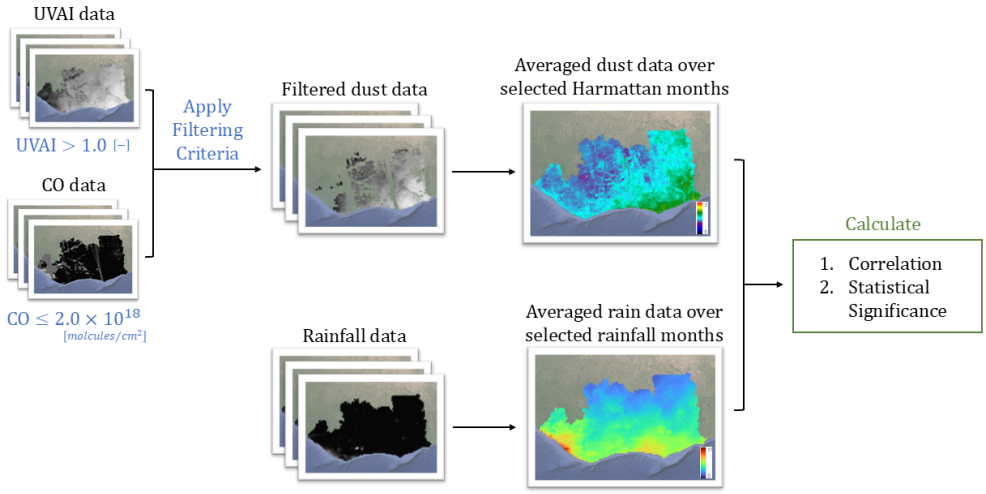

Figure 2: Methodology Overview: Using UVAI data and CO data from S5P/TROPOMI, filtering criteria were applied to generate dust data representing Harmattan impact. These dust data were then averaged over selected Harmattan periods. Rainfall data from IMERG were also collected and averaged over selected rainfall months. Finally, the correlation between Harmattan dust and rainfall was analyzed, and a statistical significance test was performed.

3.2. Harmattan Desert Dust Data

UVAI is a unitless measure that distinguishes UV-absorbing particles, such as desert dust, smoke, and volcanic ash, from non-absorbing particles. Positive UVAI values indicate the presence of UV-absorbing particles (Stein Zweers, 2022). To estimate the dust loading associated with Harmattan the UVAI data from the Copernicus S5P/TROPOMI level 3 gridded dataset were used. This quality-assured product was derived from filtered level 2 data and re-gridded onto a fixed global grid of 8193 × 16385 pixels,

with spatial resolution of approximately $0.022^\circ \times 0.022^\circ$ (European Space Agency). The data were available from May 2018, and data up to March 2025 were used. In this study, UVAI daily data were averaged using a three-day moving window to reduce variability and appearance of too many missing values.

UVAI is calculated using observations at two near-UV wavelengths (354 and 388 nm), where ozone absorption is small. The index is derived by computing the residual between the ratio of the measured top of the atmosphere reflectance and the ratio of theoretical Rayleigh scattering-only reflectance, at these wavelengths (Stein Zweers, 2022; Torres et al., 2020).

UVAI captures all types of UV-absorbing aerosols, while this study focuses specifically on desert dust. The biomass burning of agricultural waste and wildfires in the dry season of West Africa contribute to the high aerosol loading, coinciding with the Harmattan period (Wu et al., 2021; Andreae, 2019; Kabo-bah et al., 2019). To isolate desert dust from other UV-absorbing aerosols, the classification of aerosol subtypes used in the calculation of Aerosol Optical Thickness and Single Scattering Albedo in the TROPOMI product was applied. Desert dust aerosols were identified based on thresholds using UVAI values and carbon monoxide (CO) concentrations (de Graaf, 2024):

$$\text{UVAI} > 1.0 \quad [-] \quad \text{and} \quad \text{CO} \leq 2.0 \times 10^{18}\,[\text{molecules/cm}^2]$$

CO data were obtained from the S5P/TROPOMI Level 2 product, using the total CO column [mol/m^2] (Apituley et al., 2024; Borsdorff et al., 2022). The data were averaged using the same three-day moving window as the UVAI data. After applying the filtering criteria, the remaining UVAI data were considered to represent desert dust. Several comparisons with other datasets were performed to assess whether the filtered UVAI is a good representation of Harmattan strength. Specifically, Aerosol Optical Depth (AOD) data from AERONET and visibility data from the National Oceanic and Atmospheric Administration (NOAA) were used to assess whether S5P/TROPOMI UVAI captures the key characteristics of Harmattan impacts, which are shown in Appendix B. For the calculation of the correlation coefficients, the UVAI values were averaged over the selected months per pixel.

3.3. Rainfall Data

For rainfall, Integrated Multi-satellitE Retrievals for the Global Precipitation Measurement (GPM) mission (IMERG) daily precipitation data was

used. IMERG is a satellite-based rainfall estimate based on combinations of various global precipitation datasets, with a high spatial temporal resolution of approximately $0.1^\circ \times 0.1^\circ$ (Huffman et al., 2023). The research-quality gridded daily data of the IMERG Final Run were used for the period only up to November 2024 because of data availability. For early rainfall data of 2025, IMERG Late Run data were used to fill the gap. IMERG Final Run data have been adjusted and quality controlled, resulting in better accuracy, completeness, and consistency over time compared to the IMERG Late Run.

To calculate the correlation per pixel, the rainfall data was refined to align with the UVAI data. The refinement was carried out by overlaying a grid matching the spatial resolution of the dust data onto the rainfall data and extracting the nearest corresponding rainfall values. Then, daily precipitation was averaged over the entire selected rainfall months per (refined) pixel.

Using the six or seven years (six for temporal pairs with full rainfall, April-September, and seven for temporal pairs with early rainfall, April-May, due to the availability of rainfall data up to May for the year 2025) of seasonally paired dust and rainfall data (2019 – 2025), Pearson's r correlation coefficients were calculated and visualized to assess the relationship between Harmattan dust and subsequent rainfall patterns.

3.4. Significance Assessment of Correlation Coefficients

After computing the correlation coefficients for each pixel, their statistical significance was assessed using a two-tailed t-test for the Pearson correlation coefficient (Obilor and Amadi, 2018):

$$t_{\text{statistic}} = r \cdot \sqrt{\frac{n-2}{1-r^2+10^{-10}}} \tag{1}$$

r represents the correlation coefficient and n represents the degrees of freedom. The t-statistic is a measure of how far the observed Pearson correlation r is from 0.

Using the calculated t-statistics, the corresponding p-values were obtained as:

$$p = 2 \cdot (1 - F_t(|t_{\text{statistic}}|;\, \text{df} = n-2)) \tag{2}$$

Finally, statistical significance was evaluated based on the p-values. The p-value represents the probability that a given correlation r will occur if

the true correlation were actually zero. Due to the small sample size of examined years, different levels of statistical significance at 80% ($\alpha = 0.2$), 90 % ($\alpha = 0.1$), 95 % ($\alpha = 0.05$), and 99 % ($\alpha = 0.01$) were tested and visualized:

$$\text{significance} = p \leq \alpha \tag{3}$$

4. Results

Four different temporal combinations of Harmattan dust and subsequent rainfall periods were investigated in this study. However, the impact of late Harmattan (February-March) to subsequent early rainfall (April-May) was found to be the most prominent, and hence the analysis of the results in the main study will focus on this temporal pair. The results of other temporal combinations can be found in Appendix C.

The spatial distributions of the calculated Pearson's r correlation coefficients between late Harmattan (February-March) and early rainfall (April-May) across Liberia, Côte d'Ivoire, and Ghana over a seven-year period (2019-2025) are shown in Figure 3a for positively correlated areas and in Figure 3b for negatively correlated areas.

Positive correlations were generally observed in the southern part of the study area. These correlations were particularly strong in the southwest, within the latitude range of 4.25°N to 6°N and the longitude range of 4.5°W to 9°W, the southwest parts of Côte d'Ivoire and southern Liberia. In contrast, negative correlations were found in the northern parts of the study area, especially in the central to northwestern areas of both Côte d'Ivoire and Ghana, as well as northern Liberia. Overall, areas between 6°N and 8°N exhibited weaker correlation.

Figure 4 shows the results of the statistical significance of the correlation coefficients, with confidence levels of 80, 90, 95, and 99 % (Figure 4a for the positively correlated areas and Figure 4b for the negatively correlated areas). The areas with high positive correlations in the southwestern Côte d'Ivoire and southern Liberia, and parts of high negatively correlated areas in the northwestern regions of Côte d'Ivoire and northwestern to central Ghana exhibited high statistical significance. While statistically significant positive correlations were concentrated in the southwestern coastal areas, statistically significant negative correlations were more widely distributed

across the northern region. However, most of the study area showed low statistical significance overall.

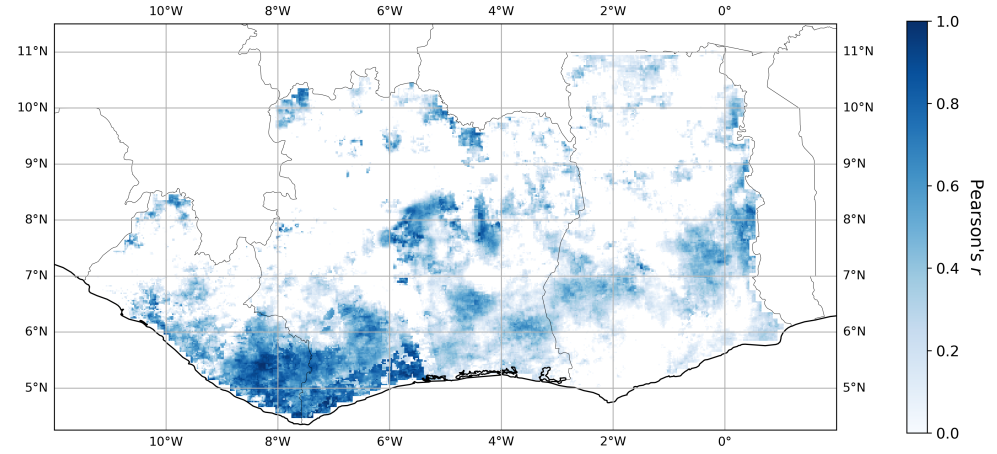

(a) Positive correlation

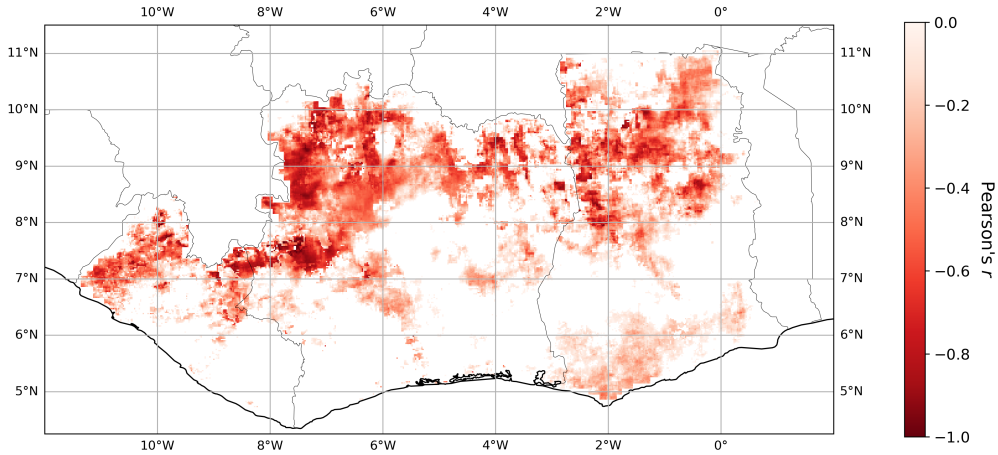

(b) Negative correlation

Figure 3: Calculated Pearson's r correlation coefficients across Liberia, Côte d'Ivoire and Ghana for late Harmattan dust (February-March) and early rainfall (April-May) for (a) positive correlation and (b) negative correlation.

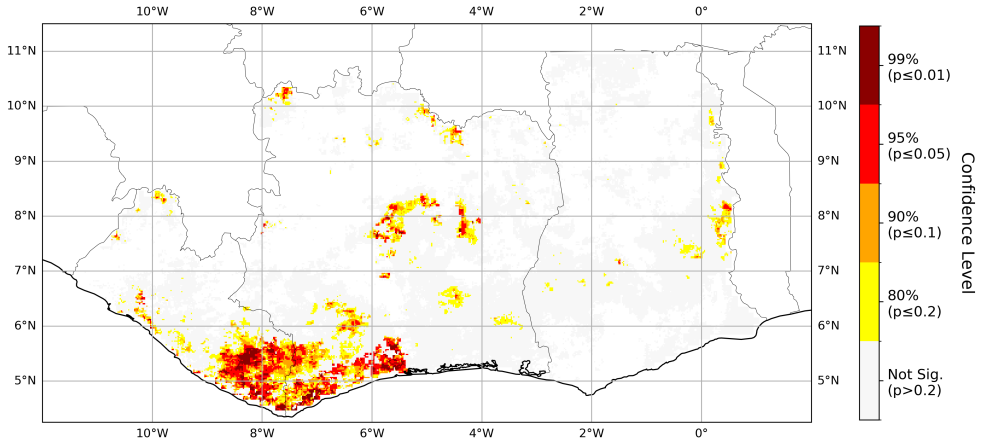

(a) Positively correlated areas

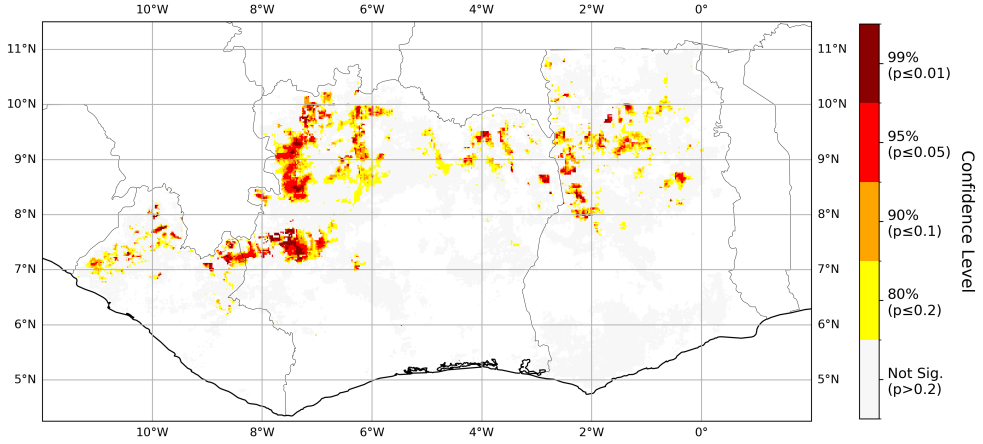

(b) Negatively correlated areas

Figure 4: Statistical significance levels (80%, 90%, 95%, 99%, and not significant) for the Pearson's r correlation between late Harmattan dust (February–March) and early rainfall (April–May) across Liberia, Côte d'Ivoire, and Ghana, for areas with (a) positive and (b) negative correlations.

The relationship between the mean February-March dust and the mean April-May rainfall for pixels with confidence levels of above 90 % are presented for positive correlation in Figure 5a and for negative correlation in Figure 5b. Data points are color-coded by year to indicate changes in distribution over time.

In the positively correlated areas, a strong relationship of Pearson's $r = 0.716$ was observed. The trend line with a slope of 3.678 indicates that the

higher dust loads in February-March are associated with higher rainfall in April-May. Year-to-year variation supports this trend: 2023 exhibited the highest mean (UV)AI values and correspondingly higher rainfall, while 2021 exhibited lowest mean AI values and lower rainfall. The mean AI values had a range of approximately 1.0 to 2.3 [-] and the mean rainfall values had a range of approximately 1.5 to 9.1 [mm/d].

The negatively correlated areas exhibited a much noisier and weaker relationship with Pearson's r = -0.333. The slope of the trend line is -2.203, smaller in magnitude compared to the positive correlation. Similar distributions were observed across the years, with less distinct year-to-year variation. April-May rainfall showed a wider range for lower AI values. The greatest variability was observed in 2025, which may be due to the use of IMERG Late data instead of IMERG Final data like other years, potentially introducing more uncertainties. The mean AI values had a narrower range of approximately 1.0 to 1.8 [-], compared to those of the positively correlated pixels. The mean rainfall values had a slightly wider range of approximately 1.3 to 9.5 [mm/d] compared to those in the positively correlated pixels.

The variations in the late Harmattan dust and early rainfall season over the years for a single pixel can be found in Appendix D. The examples of the most strongly correlated pixels for positive and negative are shown there.

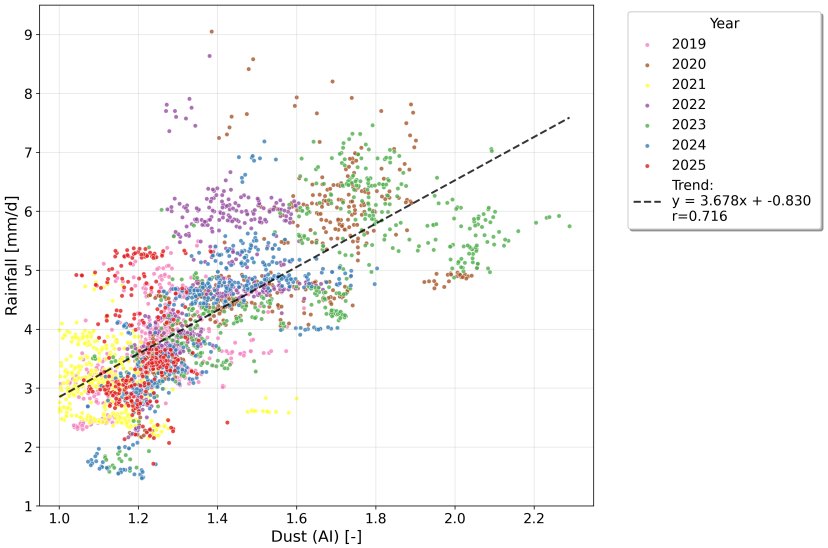

(a) Pixels with above 90% confidence level positive correlations. The dashed black line indicates the linear regression trend (y = 3.678x − 0.830), with a Pearson's correlation coefficient of $r = 0.716$.

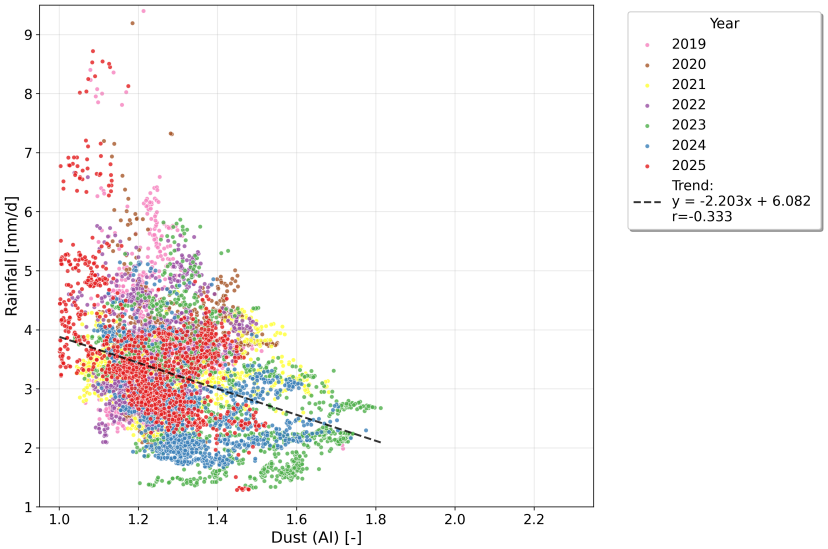

(b) Pixels with above 90% confidence level negative correlations. The dashed black line indicates the linear regression trend (y = -2.203x + 6.082), with a Pearson's correlation coefficient of $r = -0.333$.

Figure 5: Relationship between February–March mean dust, represented by Aerosol Index (AI), and April–May mean rainfall for pixels with (a) statistically significant positive correlations ($p < 0.10$) and (b) statistically significant negative correlations ($p < 0.10$) across all years (2019–2025). Each point represents a spatially averaged value for a given year, color-coded by year.

Figure 6 shows the spatial distribution of the mean dust in February-March and April-May, and the mean rainfall over April-May. The years 2021 and 2023 are taken as examples to highlight seasonal variability. Focusing on the southwestern parts of Côte d'Ivoire and southern Liberia, where strong positive correlations were observed, 2021 exhibited a low dust load in February-March (panel a) and correspondingly low April-May rainfall (panel c). Conversely, in the same area, 2023 showed a high dust load in February-March (panel d) and correspondingly high April-May rainfall (panel f), especially near the coast. Inverse patterns were observed in April-May dust levels. In 2021, the dust load in April-May remained high (panel b), whereas in 2023, the dust load was significantly reduced (panel e). This indicates that the dust load is not simultaneously high when rainfall intensifies in April–May, at least as observed by the S5P/TROPOMI satellite. The spatial distributions for all years (2019-2025) can be found in Appendix E.

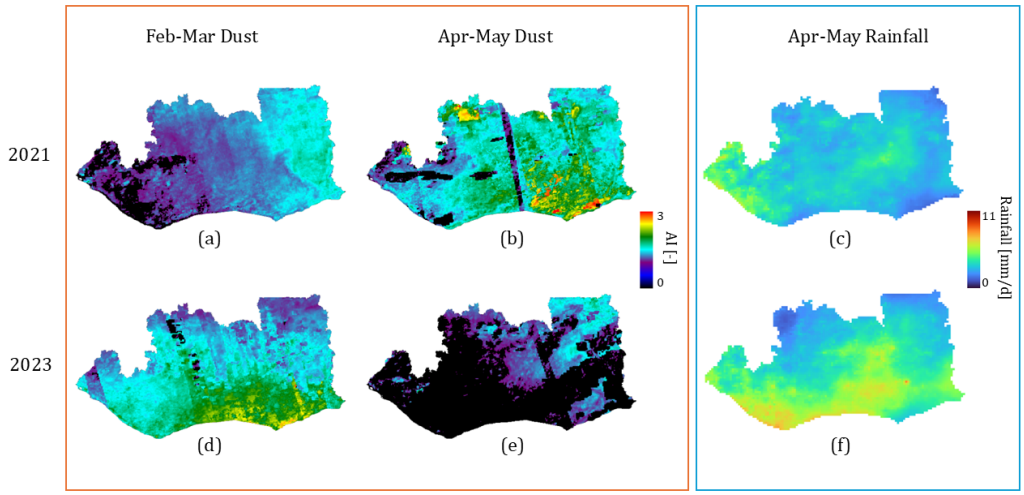

Figure 6: Spatial distribution of the mean dust, represented by (Ultra Violet (UV)) Aerosol Index (AI), for February–March (panels a and d) and April–May (panels b and e), and mean rainfall for April–May (panels c and f) over the study area. The years 2021 (panels a, b, and c) and 2023 (panels d, e, and f) are shown as examples to illustrate seasonal variations in dust loading and rainfall.

5. Discussion

5.1. Correlation between late Harmattan dust and early rainfall in the rainy season

Strong positive correlations between late Harmattan and early rainfall were observed in the southwestern Côte d'Ivoire and southern Liberia. This aligns with anecdotal evidence from a local farmer that dustier Harmattans were followed by higher precipitation in the subsequent rainy season, although this study focused only on early rainfall. The local farmer is from Gagnoa, Côte d'Ivoire, which falls under the positively correlated area found in this study. In contrast, the central to northwestern parts of Côte d'Ivoire and Ghana exhibited negative correlations, meaning that a higher dust load during a stronger late Harmattan leads to less precipitation in the early rainy season.

From the pixel-wise relationships between Harmattan dust and rainfall for areas with more than 90 % significance in Figure 5, positively correlated areas exhibited stronger correlations and less variance compared to negatively correlated areas. Similarly, the year-to-year variations were more distinct in the positively correlated areas, meaning that the data points tended to cluster by year. For example, 2021 experienced less Harmattan dust and had correspondingly low early rainfall clustered at the bottom-left of the graph. On the contrary, 2023 experienced high Harmattan dust and had correspondingly high early rainfall, clustered more in the upper right of the graph. In negatively correlated areas, the dust load remained relatively consistent across the years in a similar range of AI values. These findings suggest that in positively correlated areas, as seen mostly in the southwest of the study area, the years with stronger Harmattan are more reliably associated with more early rainfall. This relationship appears to be more robust compared to negatively correlated areas found in the northern regions, because the inverse relationship of stronger Harmattan leading to less early rainfall was weaker and less consistent.

As shown in Figure 6, high dust loads and high rainfall are unlikely to occur simultaneously. For example in 2021, when dust was still retained in April-May, rainfall remained low in April-May. In 2023, high dust load in February-March was followed by high rainfall in April-May. The dust load had declined significantly by then at the areas with high rainfall. This may indicate that due to rainfall, the dust in the atmosphere is washed away. Alternatively, there may be an opposite relation that high dust level

retentions into the rainfall season may suppress rainfall. Observations over a longer period are required to confirm these dust and rainfall relationships, and underlying mechanisms require further investigation.

Some studies mention that desert dust acting as cloud condensation nuclei can suppress rainfall activity (Rosenfeld et al., 2001; Rosenfeld and Nirel, 1996). Although Saharan dust can function as nuclei (Twohy et al., 2009; Brunner et al., 2021), it remains unclear whether the dust observed in this region functions as effective nuclei and, if so, whether that impacts the early rainfall. Whether or not the negative correlations in the northern region found in this study come from the suppressing effect of desert dust acting as cloud nuclei also needs further investigation.

In addition to dust dynamics, moisture availability may also contribute to the observed strong positive correlations in the south and negative correlations in the north. The moisture source in West Africa during the monsoon season includes both local evaporation and advection from the Gulf of Guinea (Gong and Eltahir, 1996). This moisture from the Gulf of Guinea is transported inland as the monsoon proceeds (Fink et al., 2017). At the Intertropical Discontinuity (ITD), convergence occurs between dry Harmattan winds and moist southwesterlies in the lower atmosphere, triggering rainfall (Berthou et al., 2019). This convergence zone progresses northward as the monsoon season advances. As this study focused on early rainfall, it is possible that limited moisture availability inland in northern regions contributed to reduced rainfall, exhibiting a negative correlation.

This study assessed the effect of Harmattan primarily through the dust load observed by UVAI. Consequently, the correlation identified in this study is restricted to the relationship between dust load and rainfall, leaving room for future research to explore the direct impact of Harmattan winds on precipitation, or whether a combined wind–dust effect influences rainfall. Also, Oluleye and Jimoh (2018) have reported that the evolution of near-surface wind, variations in sea surface temperature (SST) and ITD are crucial large-scale circulation systems impacting Harmattan dust transport across West Africa. The same systems could also be influencing the subsequent rainfall patterns, independently or together with Harmattan. Therefore, future research should consider looking at large circulation patterns, such as SST and ITD, beyond the relationship between only dust loads and rainfall.

These are hypothetical explanations of the correlations found between late Harmattan dust and early rainfall, as the underlying mechanisms are highly complex and not yet fully understood. A more comprehensive under-

standing of the atmospheric system is needed to draw definitive conclusions. Nevertheless, this study still portrayed a high potential for Harmattan dust in February-March as an indicator of subsequent early rainfall in April-May, offering valuable insights for farmers in West Africa.

5.2. Influence on cocoa production

The hypothesis of this study came from anecdotal evidence from a local farmer that stronger Harmattans lead to more precipitation in the following rainy season. While rainfall reduction acts negatively on cocoa production (Adet et al., 2024; Mensah et al., 2023), excessive rainfall also leads to poor production due to the spread of fungal diseases, as experienced in 2023 (Energy & Climate, 2025). Rainfall is critical for cocoa production, and the findings of this study suggest the potential to forecast early season rainfall based on late Harmattan dust levels, which could be highly beneficial for local farming communities for better agricultural planning. In this way, the results provide scientific support for traditional knowledge. According to Yoroba et al. (2019), the cocoa production is affected by the major rainy season from April to July and the short dry season from August to September. Therefore, although this study mainly focused on early rainfall in April-May, this period contributes to the onset and total rainfall in the major rainy season. In that sense, the insights gained in this study remain highly relevant for cocoa production.

Many studies point out the vulnerability of future cocoa production due to climate change (Schroth et al., 2016; Delgado-Ospina et al., 2021). The production levels may fluctuate substantially depending on rainfall patterns and hence a better understanding of the climatic relationships is important for cocoa farmers to achieve stable production.

5.3. Limitations

One of the limitations of this study was the restricted number of years evaluated, due to the availability of S5P/TROPOMI data only from May 2018 onward. As a result, 7 years of data were assessed for the main analysis and only 6 years of data for temporal pairs with full rainfall. This reduces the robustness of the calculated correlations and introduces uncertainty. To enhance the results and acknowledge the variations of dust and rain patterns over the years, future analyses should incorporate additional years of data once they are available. Moreover, IMERG Final Run should be used instead

of IMERG Late Run for the rainfall data in 2025, in order to keep datasets consistent and for better quality data.

Also, filtering criteria were applied to UVAI to ensure that only desert dust was considered among all UV-absorbing aerosols. However, it remains uncertain whether the filtering process completely isolates dust from other UV-absorbing aerosols, and whether the average of filtered UVAI over several months would be an appropriate method to assess the impact of Harmattan dust per year.

6. Conclusion

This study investigated the relationship between Harmattan dust and precipitation in the subsequent rainy season using Sentinel-5P TROPOMI satellite data. Four seasonal pairs of Harmattan dust and rainfall periods were evaluated, with a focus on the relationship between late Harmattan (February–March) and early rainfall (April–May). The use of high-resolution satellite data enabled detailed spatial analysis, enhancing the understanding of regional climatology in West Africa. Given that correlations with large scale predictors such as El Niño with rainfall in West Africa are severely limited, this is, to our knowledge, the first promising seasonal rainfall forecast method.

The correlation analysis showed that the southwestern regions of Côte d'Ivoire and southern Liberia have a high positive correlation between late Harmattan dust and early rainfall. This finding aligns with a local belief that dustier Harmattans are followed by more precipitation. In contrast, northwestern parts of Ghana and also northern parts of Côte d'Ivoire indicated negative correlations. Several explanations may support these findings, but reality could be more complicated than the relations discussed in this study.

These findings are especially important for local cocoa farmers, as cocoa production is greatly affected by the amount of rainfall. Understanding the potential link between Harmattan dust and rainfall could support better seasonal forecasting and agricultural planning.

Overall, this study provides scientific support for local anecdotal evidence about Harmattan strength and subsequent rainfall. The use of high-resolution satellite data enabled detailed analysis, and the results highlight significant correlations in the major cocoa-producing areas. However, the physical relationship between Harmattan dust and subsequent rainfall re-

mains complex and further research is still required to obtain a more comprehensive understanding.

Appendix A. Assessing Harmattan Dust Influence on subsequent Rainfall with a Supplementary Long-Term Dataset

To assess the relationship between Harmattan dust and subsequent rainfall, a different dataset was used to look at the impact for longer periods of time and to assess the differences with using much coarser spatial resolution.

For this, the Absorbing Aerosol Index (AAI) from the Global Ozone Monitoring Experiment-2 (GOME-2) instrument and Carbon Monoxide (CO) from Measurement of Pollution in the Troposphere (MOPITT) were used to assess the dust intensity during Harmattan, also applying the same filtering method as the main study to focus on desert dust. Instead of averaging over a three-day moving window, these data were averaged over a five-day moving window as they had more missing values compared to the S5P/TROPOMI data.

The gridded data for both AAI and CO used for the analysis had spatial resolutions of $1^\circ \times 1^\circ$. The difference in resolutions between S5P/TROPOMI (UVAI) and GOME-2 (AAI) data can be compared in Figure A.7. For calculating the correlation, the filtered AAI data representing desert dust was refined to align the IMERG rainfall data. The same refining method was used as the main analysis, but this time for the dust data, by overlaying a grid matching the spatial resolution of the rainfall data onto the dust data and extracting the nearest corresponding dust values.

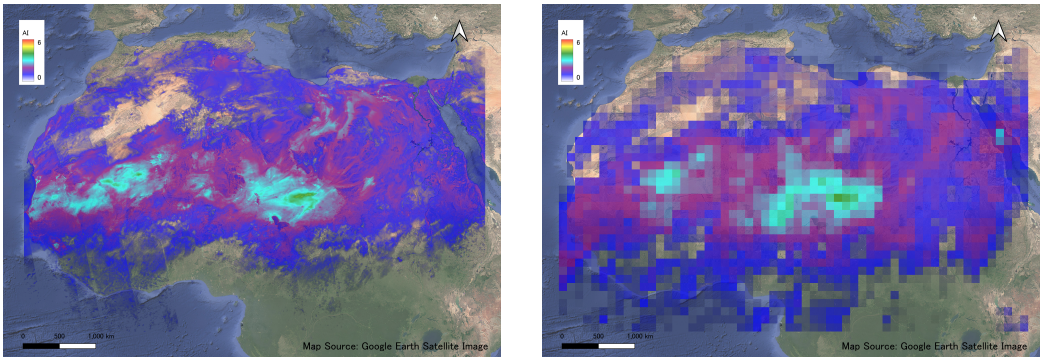

(a) S5P/TROPOMI UVAI (b) GOME-2 AAI

Figure A.7: Comparison of aerosol index (AI) products on May 1, 2020, highlighting the spatial resolution difference between (a) high-resolution S5P/TROPOMI UVAI and (b) coarser-resolution GOME-2 AAI.

Appendix A.1. Comparison of S5P/TROPOMI dataset and GOME-2 & MOPITT dataset

The differences between the S5P/TROPOMI and GOME-2 & MOPITT datasets were compared using filtered dust data of AI (UVAI and AAI).

Figures A.8a and A.9a show differences in the extent of AI and the mean values of AI classified as dust over the study area (Figure 1) between the two datasets during the overlapping period from May 2018 to September 2021. The extent of AI means the total area having positive values of AI, and the mean is averaged AI over the entire study area. The rolling averages of 14 days are shown for an easier understanding of the characteristics over time. Figures A.8b and A.9b show the calculated correlations between the two datasets during the Harmattan period from November to March, which were 0.68 and 0.65 respectively. Generally, GOME-2 & MOPITT data exhibit higher values in terms of both extent and mean. Because the spatial resolutions are quite different, changes in one grid cell in GOME-2 & MOPITT data could lead to a large difference.

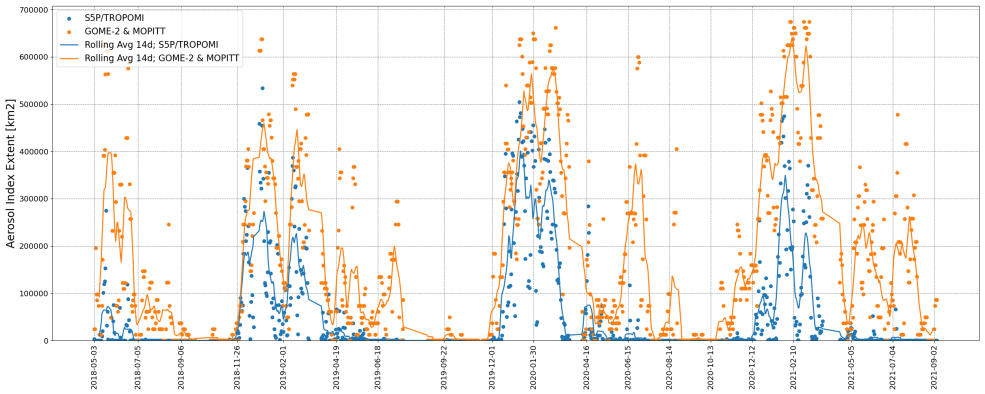

(a)

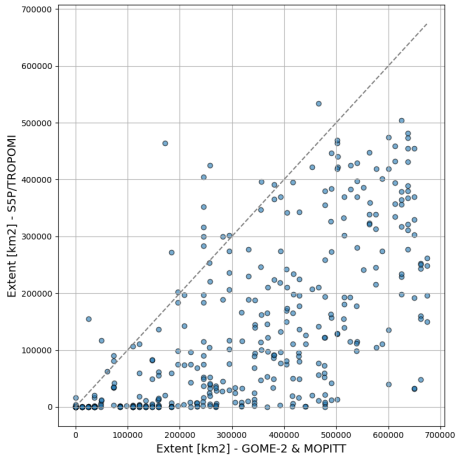

(b)

Figure A.8: Comparison of S5P/TROPOMI data and GOME2-MOPITT Harmattan dust data in terms of Extent in km^2 for study area

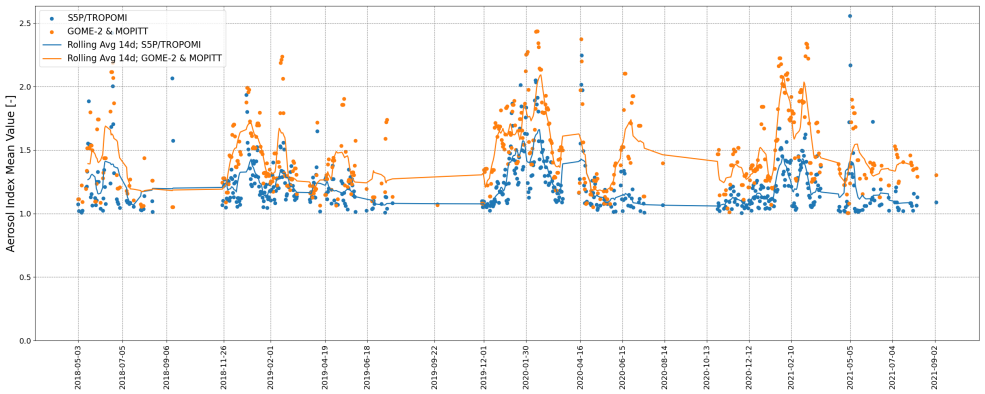

(a)

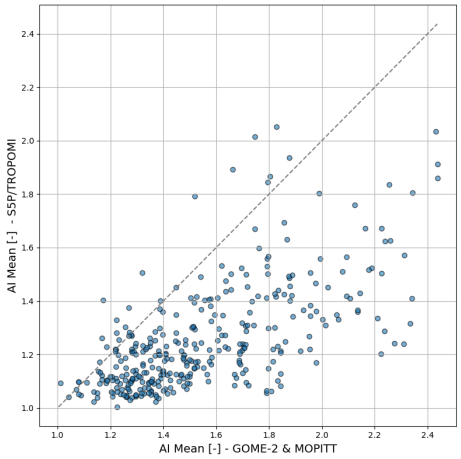

(b)

Figure A.9: Comparison of S5P/TROPOMI data and GOME2-MOPITT Harmattan dust data in terms of average UVAI values for study area

When a larger region is taken (for example as the area shown in A.10), the difference between the two datasets became smaller. Figures A.11a and A.12a show differences in the extent of AI and the mean values of AI classified as dust in the larger region over time between the two datasets during the same overlapping period from May 2018 to September 2021. Again, the rolling averages of 14 days are shown for an easier understanding of the characteristics over time. Figures A.11b and A.12b show the calculated correlations between the two datasets during the Harmattan period from November to March, which were 0.71 and 0.73 respectively. The correlations between the two datasets in terms of the extent that AI covers and the mean values over

the entire region increased as the assessed region became larger. Specifically, changes in mean AI over time follow a very similar pattern. It can be concluded that potential analysis for larger areas can be performed using coarser spatial resolution from GOME-2 & MOPITT data, but detailed analysis in smaller regions requires careful attention.

Figure A.10: A larger region of West Africa used for the analysis

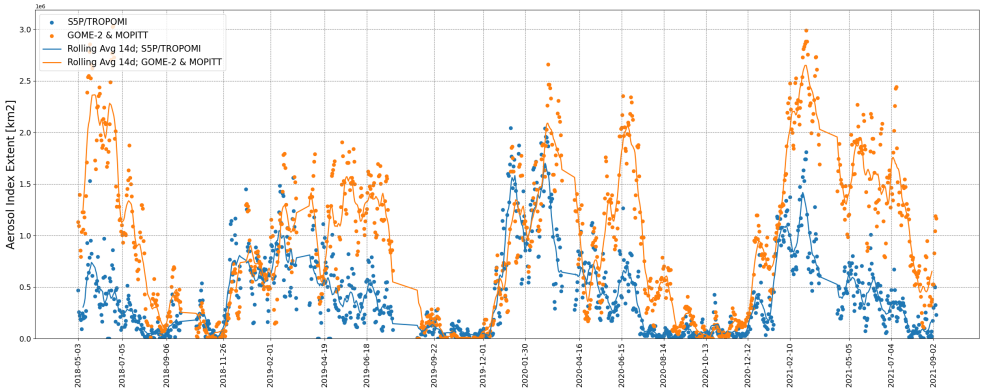

(a)

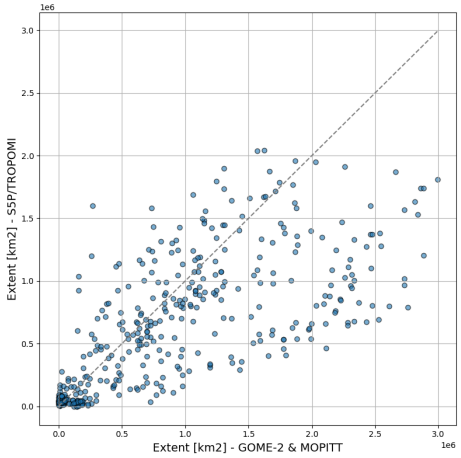

(b)

Figure A.11: Comparison of S5P/TROPOMI data and GOME-2 & MOPITT Harmattan dust data in terms of Extent in km^2 for the region shown in Figure A.10

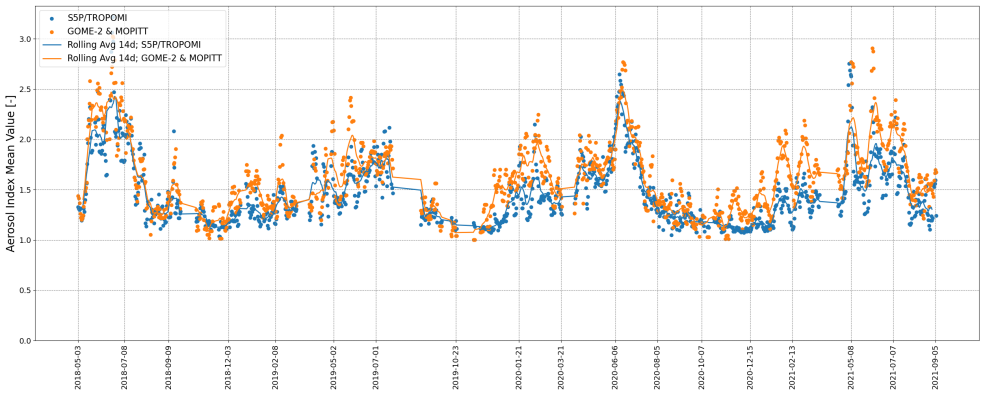

(a)

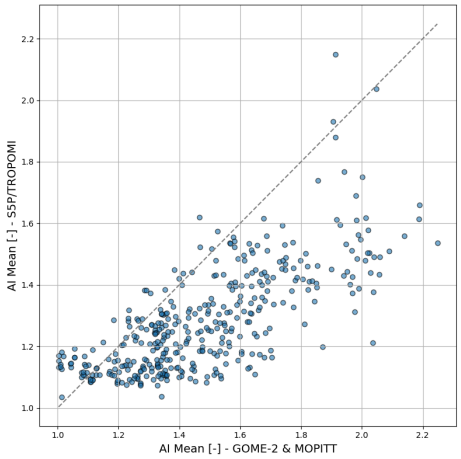

(b)

Figure A.12: Comparison of S5P/TROPOMI data and GOME2-MOPITT Harmattan dust data in terms of average UVAI values for the region shown in Figure A.10

Appendix A.2. Harmattan dust and rainfall relations

Acknowledging the lack of details due to the difference in the resolution, the correlation between Harmattan dust and subsequent rainfall for the same four seasonal pairs mentioned in the main research using GOME-2 & MOPITT data is presented.

Figure A.13 shows the correlation calculated for the impact of late Harmattan (February-March) on the subsequent early rainfall (April-May) period. A similar high positive correlation pattern was observed as the correlation with the S5P/TROPOMI data analysis in southern Liberia and southwestern Côte d'Ivoire. The northwestern regions of Côte d'Ivoire exhibit a

negative correlation, which was again observed in the S5P/TROPOMI analysis. These regions also show high statistical significance as seen in Figure A.14. However, a large part of eastern Ghana exhibits a positive correlation which is not consistent with what was observed in the main study especially in the northern regions. The reason for these differences is unknown and needs further investigation.

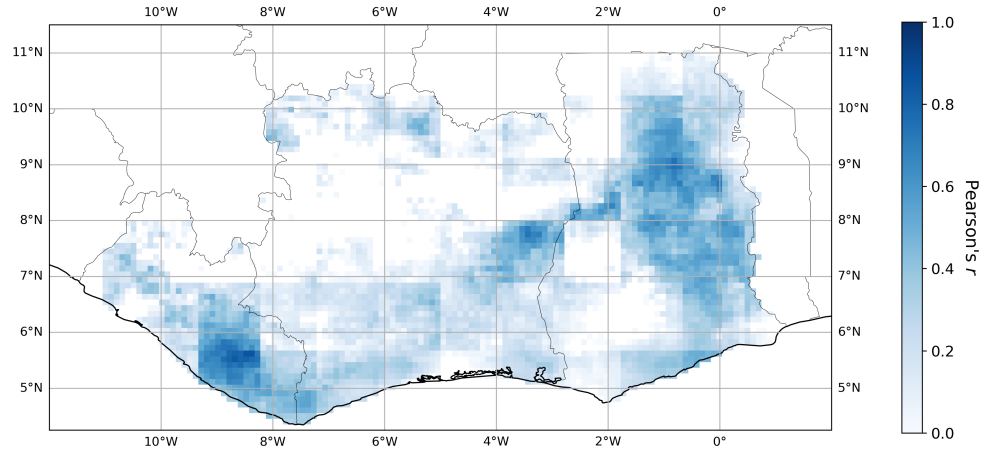

(a) Positive Correlation

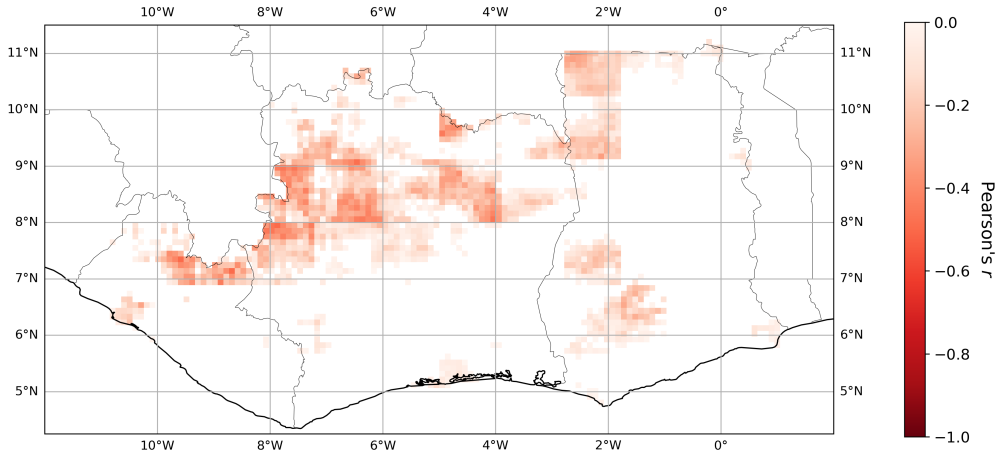

(b) Negative Correlation

Figure A.13: Calculated Pearson's r correlation coefficients using GOME-2 & MOPITT data across Liberia, Côte d'Ivoire and Ghana for late Harmattan dust (February-March) and early rainfall (April-May) for (a) positive correlation and (b) negative correlation.

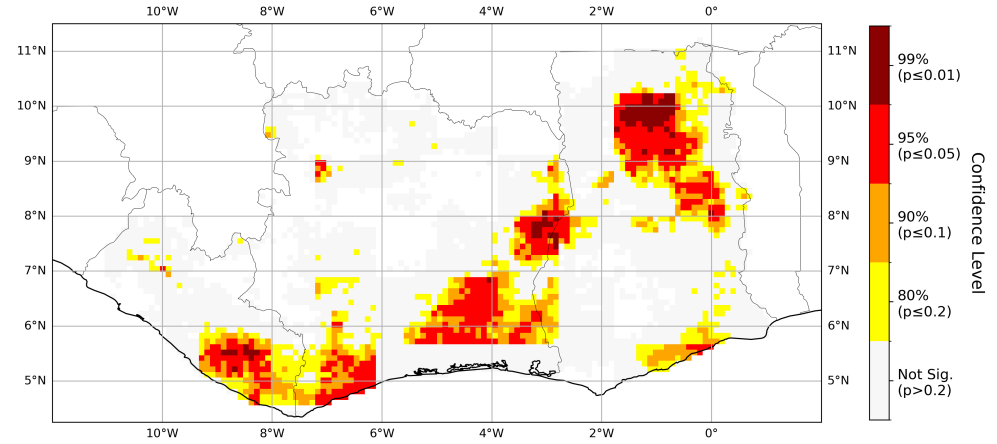

(a) Positively correlated areas

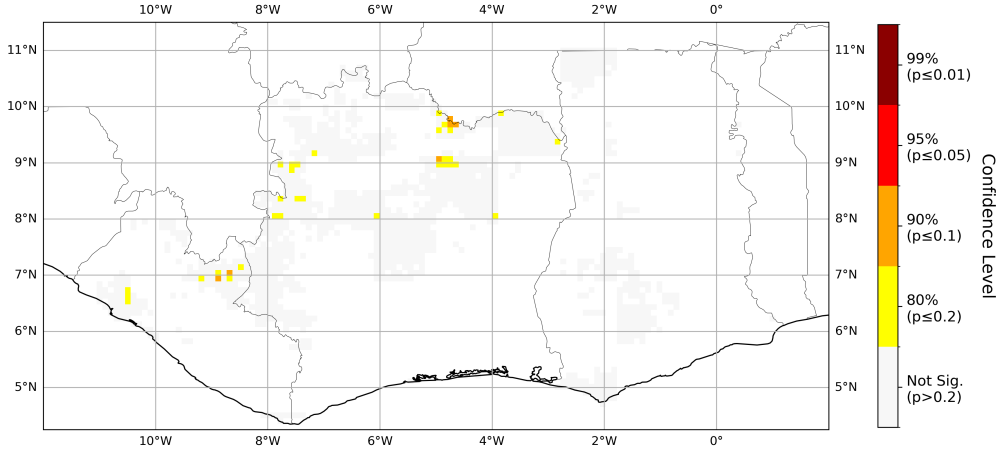

(b) Negatively correlated areas

Figure A.14: Statistical significance levels (80%, 90%, 95%, 99%, and not significant) for the Pearson's r correlation between late Harmattan dust (February–March) and early rainfall (April–May) across Liberia, Côte d'Ivoire, and Ghana, for areas with (a) positive and (b) negative correlations.

Figure A.15 shows the calculated Pearson correlation coefficients between full Harmattan (November-March) and full rainfall (April-September) using GOME-2 & MOPITT data. Positive correlations were observed almost entirely over the study area, and strong positive correlations in northeastern Ghana and eastern Côte d'Ivoire. Negative correlations are only observed weakly at the coastal regions in the south of the study area. Figure A.16b shows the corresponding statistical significant test results. High statistical

significance is observed at the highly correlated areas in northeastern Ghana and eastern Côte d'Ivoire. The very edge of the coast in Côte d'Ivoire also exhibits statistical significance.

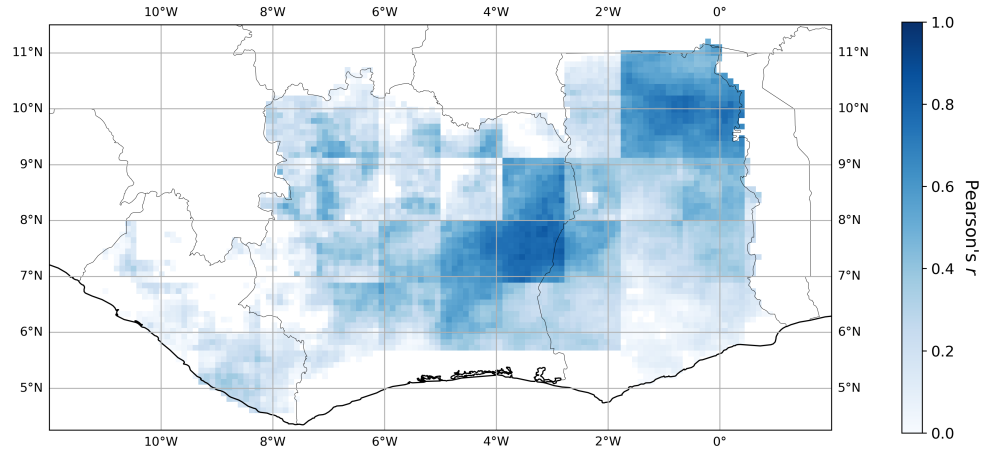

(a) Positive Correlation

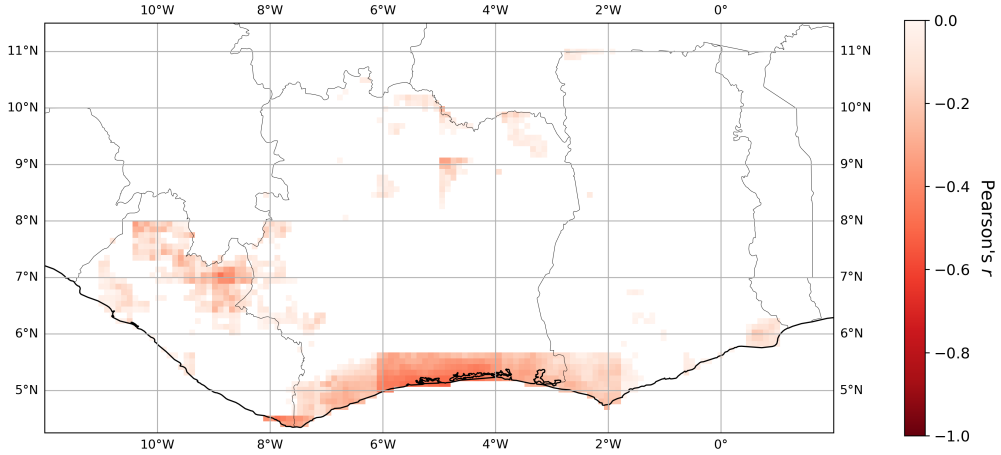

(b) Negative Correlation

Figure A.15: Calculated Pearson's r correlation coefficients using GOME-2 & MOPITT data across Liberia, Côte d'Ivoire and Ghana for full Harmattan dust (November-March) and full rainfall (April-September) for (a) positive correlation and (b) negative correlation.

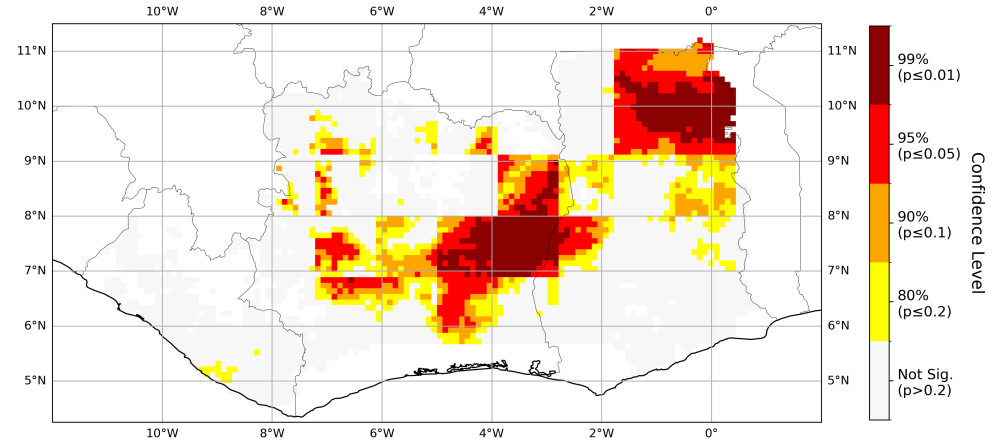

(a) Positively correlated areas

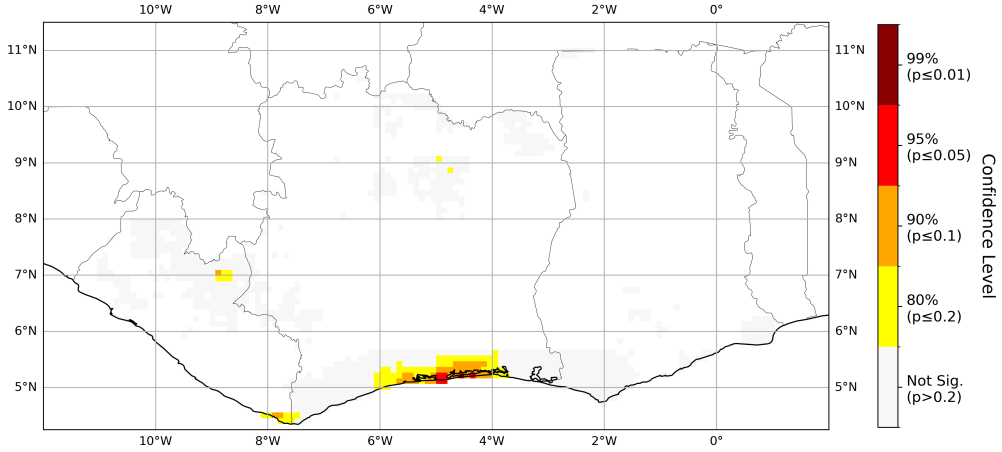

(b) Negatively correlated areas

Figure A.16: Statistical significance levels (80%, 90%, 95%, 99%, and not significant) for the Pearson's r correlation between full Harmattan dust (November–March) and full rainfall (April–September) across Liberia, Côte d'Ivoire, and Ghana, for areas with (a) positive and (b) negative correlations.

Figure A.17 shows the calculated Pearson correlation coefficients between full Harmattan (November-March) and early rainfall (April-May) using GOME-2 & MOPITT data. The correlation patterns were similar to the one found for late Harmattan and early rainfall (Figure A.13). Positive correlations were observed in the southern and eastern Côte d'Ivoire. Almost the entire area of Liberia and Ghana exhibits positive correlations as well. The correlations were strongest at southwestern Côte d'Ivoire, southern Liberia,

eastern Côte d'Ivoire, and central parts of northern Ghana. Negative correlations were observed in the northern regions of Côte d'Ivoire, although these are generally weak. Figure A.18b shows the corresponding statistical significant test results. High statistical significance was observed at the locations of high positive correlations, in southwestern Côte d'Ivoire, southern Liberia, eastern Côte d'Ivoire, and central parts of northern Ghana.

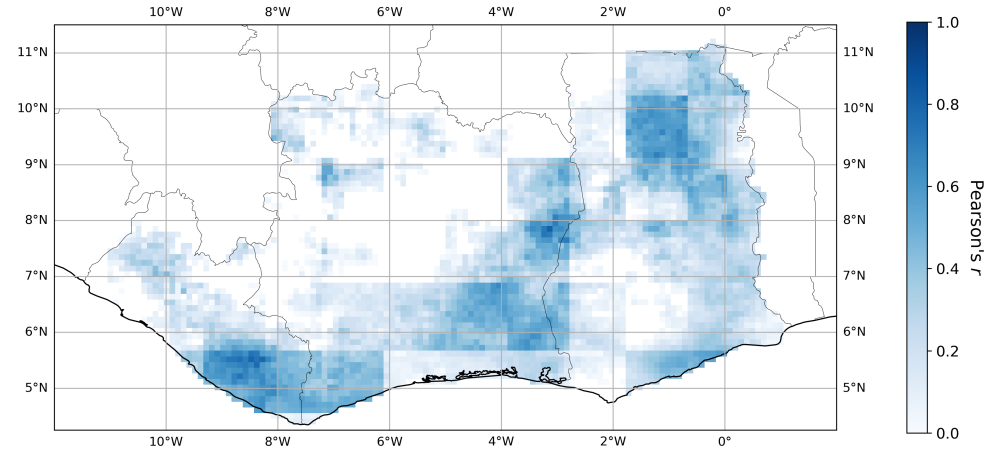

(a) Positive Correlation

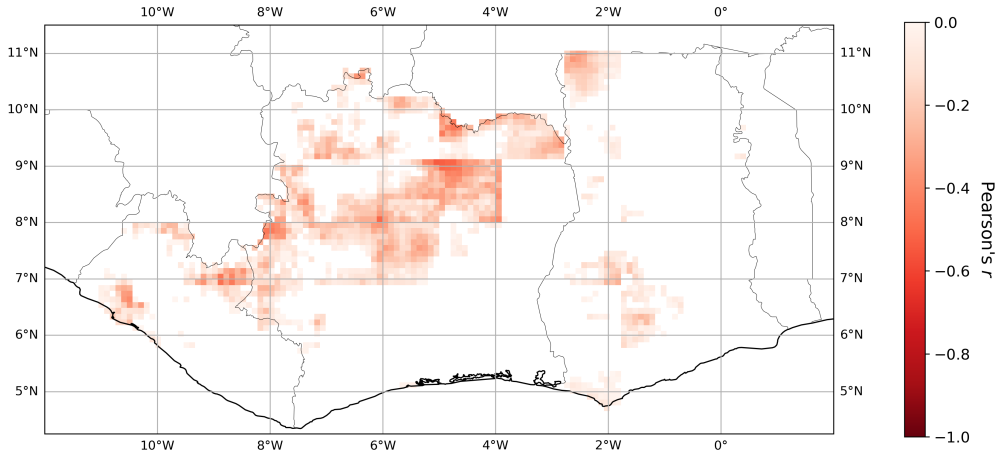

(b) Negative Correlation

Figure A.17: Calculated Pearson's r correlation coefficients using GOME-2 & MOPITT data across Liberia, Côte d'Ivoire and Ghana for full Harmattan dust (November-March) and early rainfall (April-May) for (a) positive correlation and (b) negative correlation.

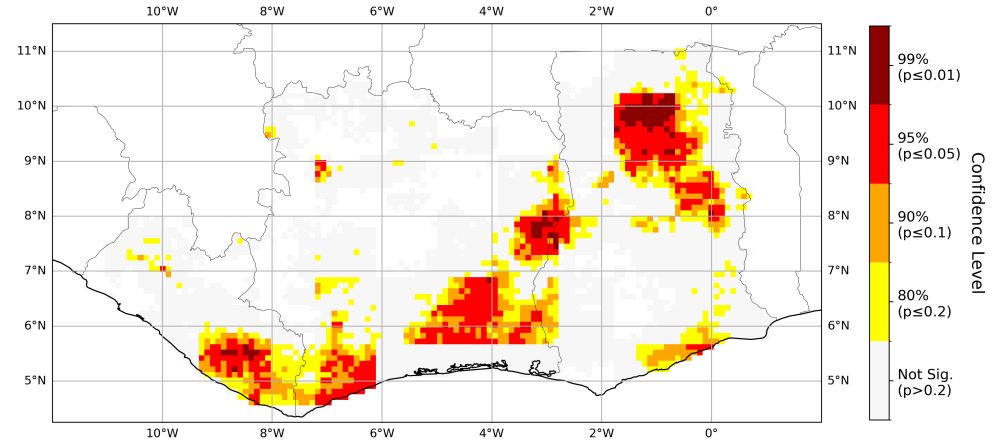

(a) Positively correlated areas

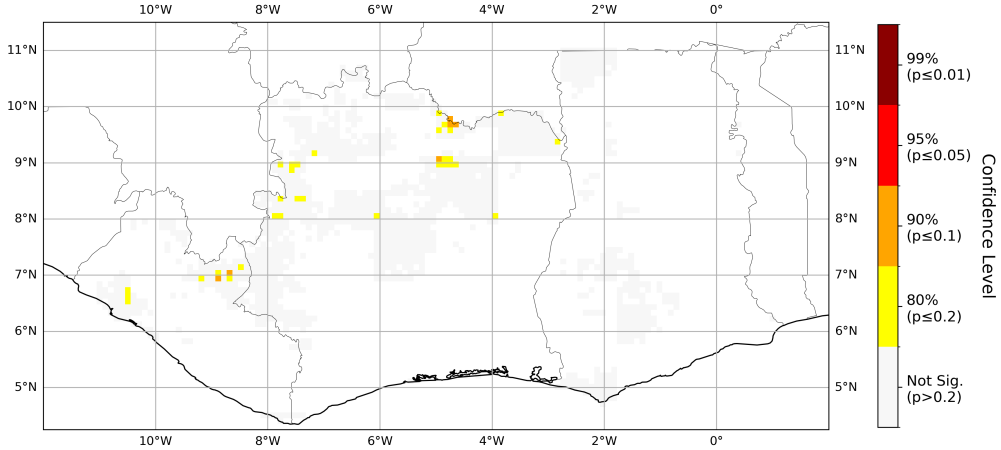

(b) Negatively correlated areas

Figure A.18: Statistical significance levels (80%, 90%, 95%, 99%, and not significant) for the Pearson's r correlation between full Harmattan dust (November–March) and early rainfall (April–May) across Liberia, Côte d'Ivoire, and Ghana, for areas with (a) positive and (b) negative correlations.

Figure A.19 shows the calculated Pearson correlation coefficients between late Harmattan (February-March) and early rainfall (April-September) using GOME-2 & MOPITT data. The correlation patterns were similar to the one found for full Harmattan and full rainfall (Figure A.15), showing positive correlations throughout study area. Some parts in the south near the coast and northern Liberia showed weak negative correlations. Figure A.20b shows the corresponding statistical significant test results. High statistical

significance was observed in northeastern Ghana, central and western Côte d'Ivoire where positive correlations were found. No statistical significance was found for negatively correlated regions.

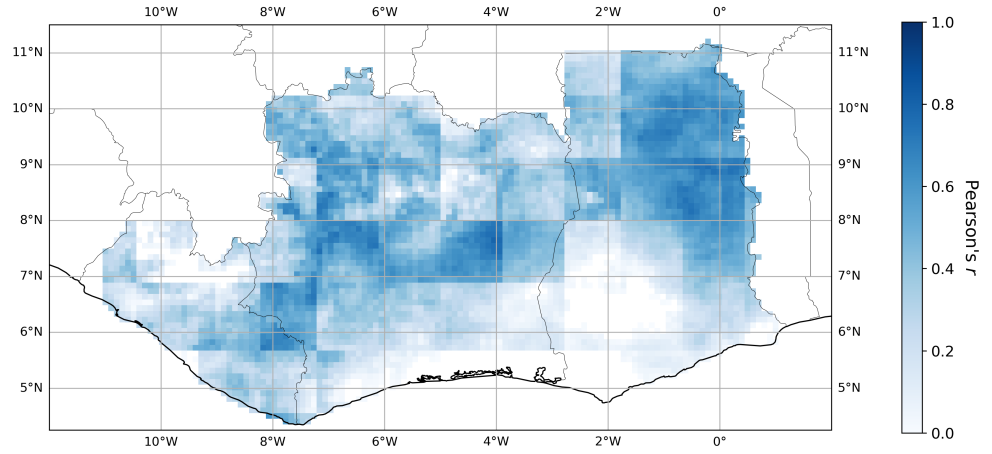

(a) Positive Correlation

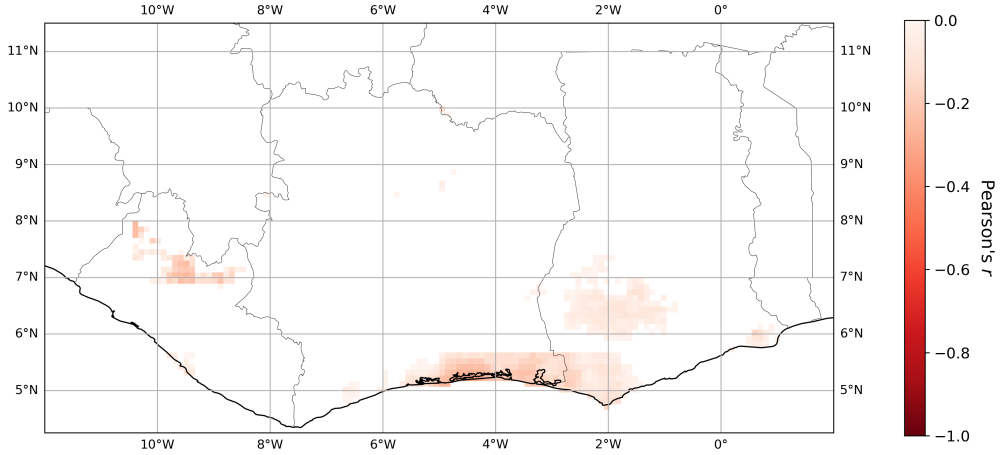

(b) Negative Correlation

Figure A.19: Calculated Pearson's r correlation coefficients using GOME-2 & MOPITT data across Liberia, Côte d'Ivoire and Ghana for late Harmattan dust (February-March) and full rainfall (April-September) for (a) positive correlation and (b) negative correlation.

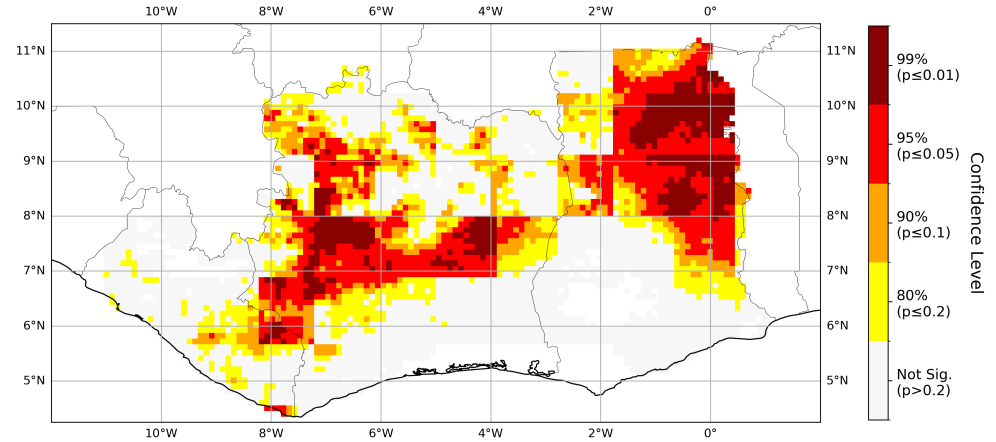

(a) Positively correlated areas

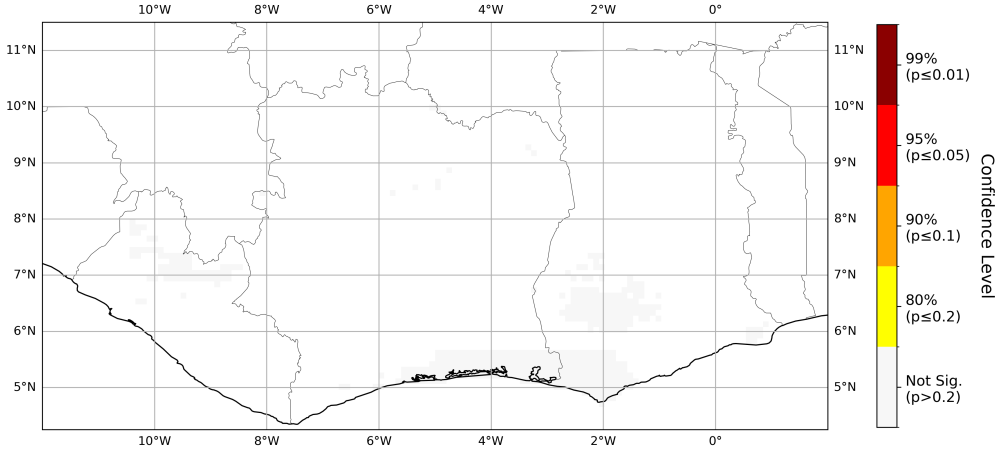

(b) Negatively correlated areas

Figure A.20: Statistical significance levels (80%, 90%, 95%, 99%, and not significant) for the Pearson's r correlation between late Harmattan dust (February–March) and full rainfall (April–September) across Liberia, Côte d'Ivoire, and Ghana, for areas with (a) positive and (b) negative correlations.

Appendix B. Evaluating the Aerosol Index as a Representation for Harmattan Impact

To assess whether the filtered UVAI values taken from S5P/TROPOMI data are good representations of Harmattan dust impact, they were compared with other datasets that could be indicative of Harmattan dust intensity.

Appendix B.1. Comparison with Aerosol Optical Depth

The filtered UVAI data were compared with Aerosol Optical Depth (AOD) data from the AErosol RObotic NETwork project (AERONET). AOD is a quantitative measure of the extinction of solar radiation by aerosol particles in the atmosphere, showing how much light is prevented from passing through because of aerosols (National Aeronautics and Space Administration). AERONET provides ground-based remote sensing data using sun photometers that measure AOD at multiple wavelengths (Giles et al., 2019). There were two AERONET stations within the study area, Koforidua in Ghana and Lamto in Côte d'Ivoire, and Level 2 Quality Assured data from these two stations were used for the analysis. For UVAI data, the mean value within a 5km radius around each station location was used. This is based on a method employed in another study comparing AOD between AERONET and MODIS datasets (Ștefănie et al., 2023).

Before the comparison, AOD data was filtered using 2D-space aerosol classification reported in Mao et al. (2019) to ensure the AOD data also represent desert dust and not other aerosols. With this filtering step, non-dust aerosol data points were removed, although most of the data points were already classified as desert dust.

Figures B.21a and B.21b show the timeseries in UVAI and AOD over the period of 2018 to 2024 for the days available for the Koforidua and Lamto stations respectively. These values have been standardized for comparison. This presents that UVAI increases around the same time as AOD increases during the Harmattan periods, though the missing data introduce uncertainties.

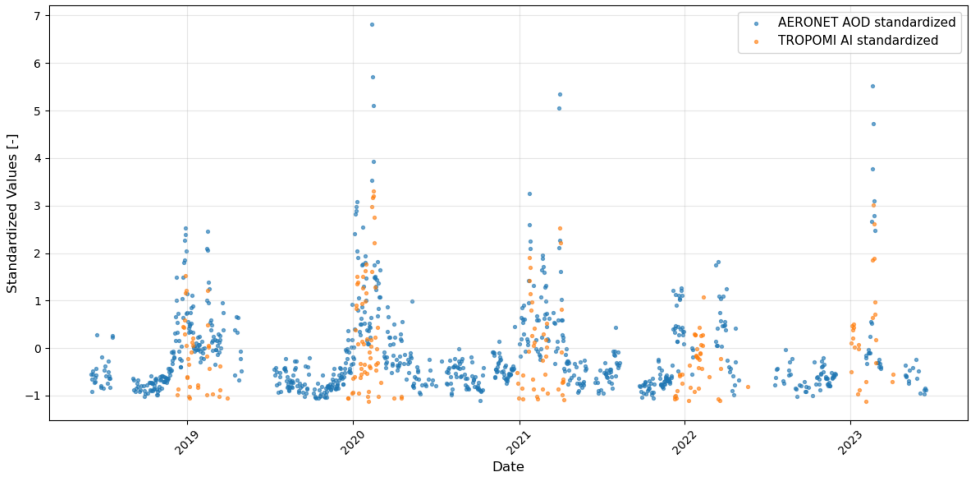

(a) Koforidua station

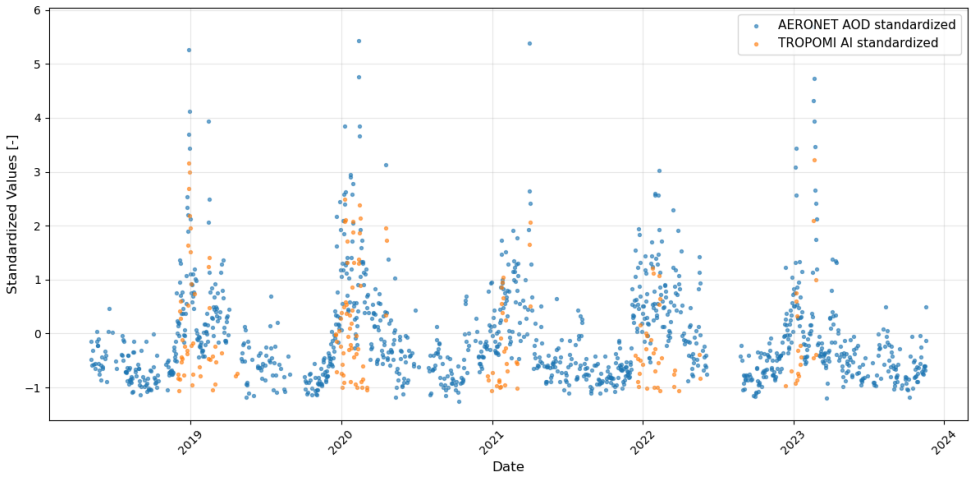

(b) Lamto station

Figure B.21: Comparison of changes in AERONET AOD and TROPOMI UVAI over time. Both data have been standardized for comparison [-].

Figures B.22 and B.23 illustrate the correlation between standardized UVAI and AOD values on the matching dates for the Koforidua and Lamto stations in (a), and (b) show the monthly mean values from December to March. Monthly means were compared to address gaps in daily data, as well as to align with analysis in the main study being conducted in monthly means. December to March was selected to account for the Harmattan periods, November was excluded due to an insufficient number of data points

though this was included in the main study.

At the Koforidua station, the daily correlation yielded a Pearson correlation coefficient of 0.80, while the monthly correlation was slightly higher at 0.82. At the Lamto station, the daily and monthly correlation coefficients were 0.62 and 0.75, respectively. These results indicate a strong positive correlation between AOD and UVAI, suggesting that UVAI obtained from S5P/TROPOMI data effectively captures the presence and variability of Harmattan dust.

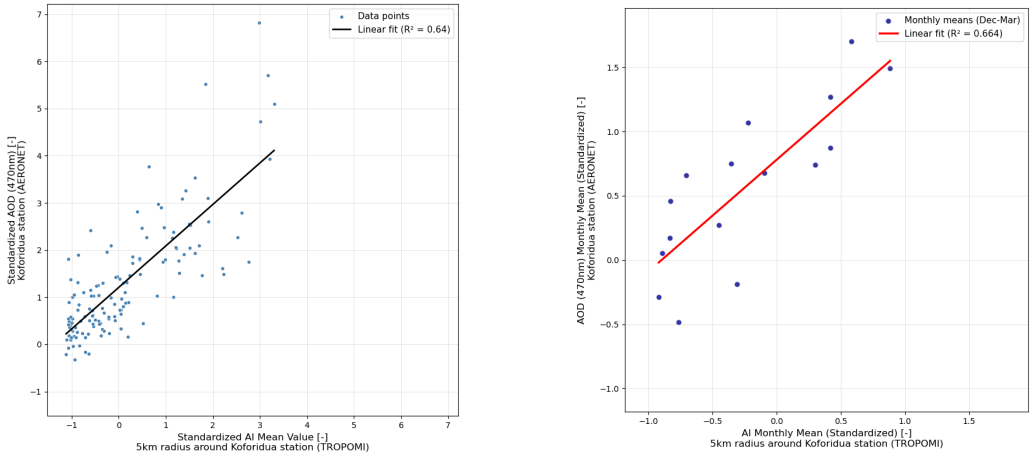

(a) (b)

Figure B.22: Comparison of UVAI data from S5P/TROPOMI and AOD data from AERONET at Koforidua station, Ghana: (a) daily data, (b) averaged monthly data for the months in December to March

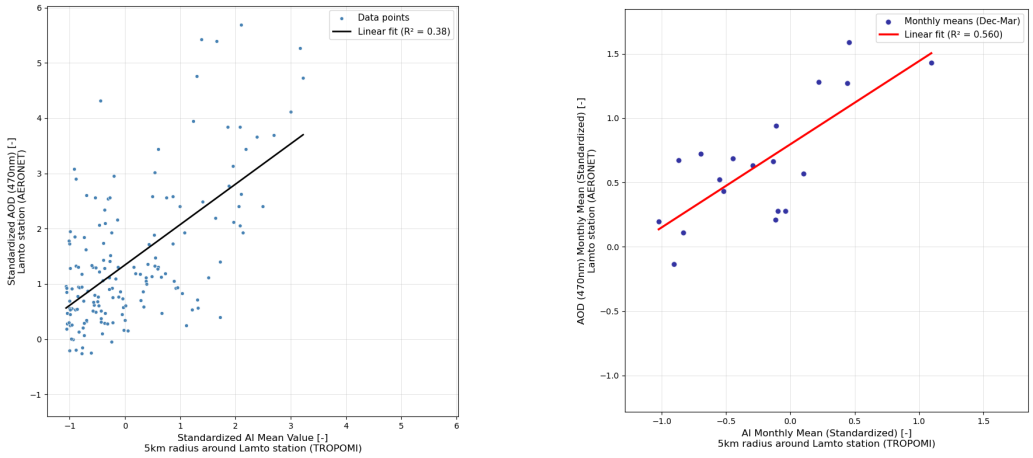

(a) (b)

Figure B.23: Comparison of UVAI data from S5P/TROPOMI and AOD data from AERONET at Lamto station, Ghana: (a) daily data, (b) averaged monthly data for the months in December to March

Appendix B.2. Comparison with Visibility

The filtered UVAI data were also compared with the visibility data for the Koforidua station. The same 5 km radius mean data were used for UVAI. The visibility data from Global Surface Summary of the Day were obtained from the National Oceanic and Atmospheric Administration (NOAA), which records the visibility in miles. Figure B.24 shows the correlation between UVAI from S5P/TROPOMI and the visibility data for daily and monthly correlations (December-March). The daily correlation yielded a Pearson correlation coefficient of -0.53, while the monthly correlation was slightly weaker at -0.51. This shows a moderate correlation that when the UVAI value is high, the visibility decreases. In another study comparing the values of TOMS AI and visibility, the correlation was much higher during Harmattan (Anuforom et al., 2007). One of the reasons why this correlation was weaker could be due to the fact that the visibility data was not filtered. Hence, the visibility data include all kinds of aerosol impact, while the filtered UVAI data represent only the desert dust. In the previous study with the TOMS AI comparison with visibility, the TOMS AI values were not treated and included all types of absorbing aerosols. Also, the product documentation mentions: "For some stations/countries, the visibility will sometimes 'cluster' around a value (such as 10 miles) due to the practice of not reporting visibilities greater than

certain distances" (NATIONAL CENTERS FOR ENVIRONMENTAL INFORMATION, 2020). Therefore, the quality of the data may be unreliable on certain days.

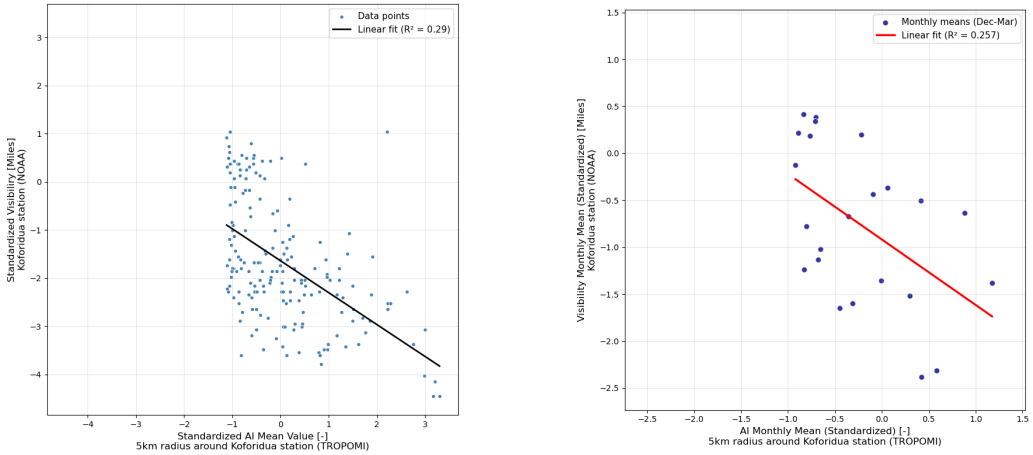

(a) (b)

Figure B.24: UVAI vs. Visibility at Koforidua station, Ghana

Appendix C. Results of different temporal pairs of Harmattan dust and subsequent rainfall periods

Here, three of the four seasonal pairs of Harmattan dust and subsequent rainfall that were not included in the main study are presented. Although correlation can be found in these temporal pairs as well, averaging over a long period of time could cause significant uncertainties and more years of data is needed to understand the relations further.

Appendix C.1. Full Harmattan to Full rainfall

Figure C.25 shows the correlation between full Harmattan (November-March) and full rainfall (April-September). High positive correlations were observed in the southwestern regions of Côte d'Ivoire and southern Liberia, resembling those found in the seasonal pair of late Harmattan and early rainfall, though weaker in magnitude. Positive correlations were observed in the northern and central regions in Côte d'Ivoire, as well as regions above 7 °N in Ghana. In contrast, high negative correlations were observed in northern Liberia, northwestern Côte d'Ivoire, and southern Ghana. Figure C.26 shows

the statistical significance of the calculated correlations. Southern regions in Liberia and northern regions in Côte d'Ivoire in the positively correlated area showed high statistical significance. Parts of western Côte d'Ivoire, parts of northern Liberia, and southeastern Ghana in the negatively correlated area showed high statistical significance, but only in limited regions.

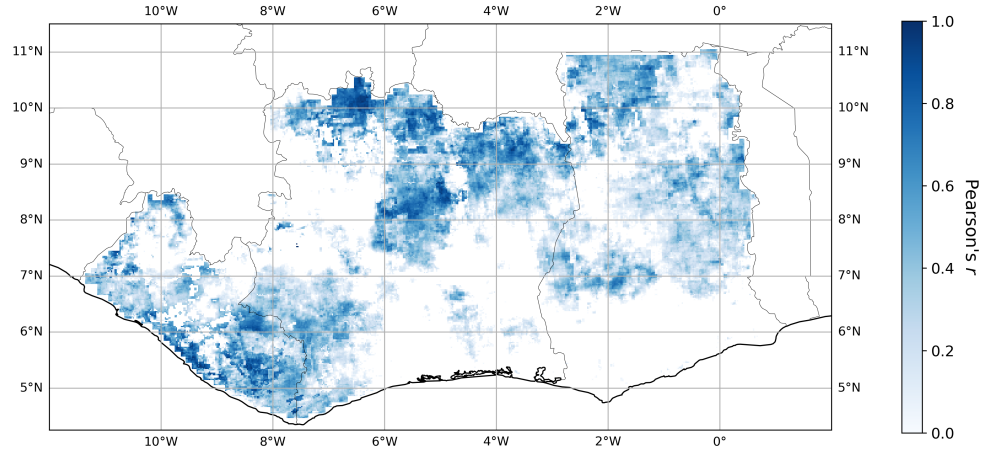

(a) Positive Correlation

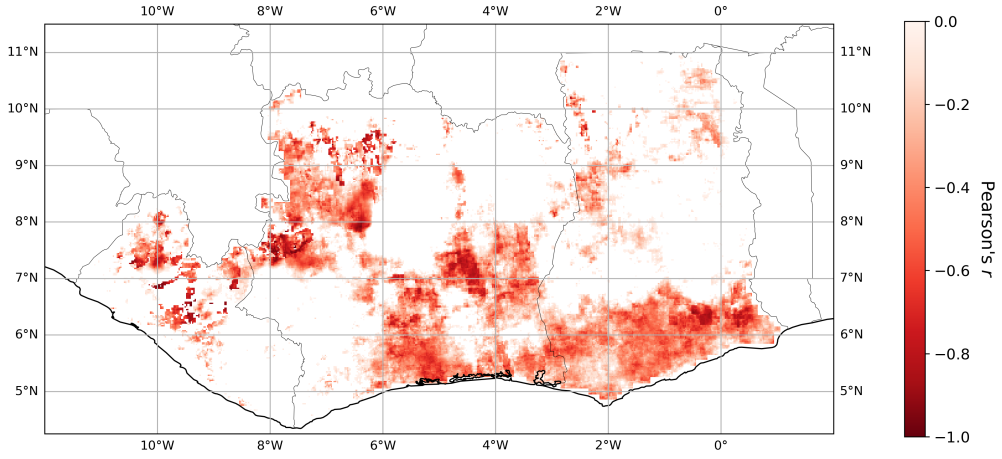

(b) Negative Correlation

Figure C.25: Calculated Pearson's r correlation coefficients across Liberia, Côte d'Ivoire and Ghana for full Harmattan dust (November-March) and full rainfall (April-September) for (a) positive correlation and (b) negative correlation.

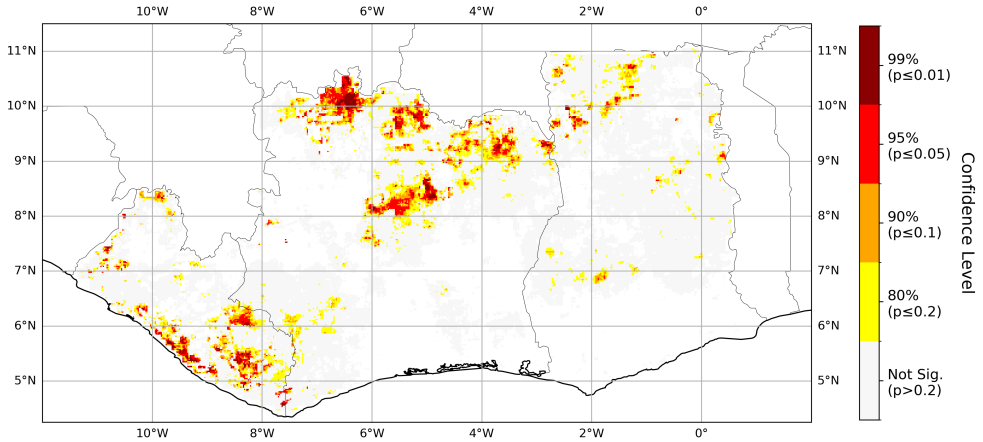

(a) Positively correlated areas

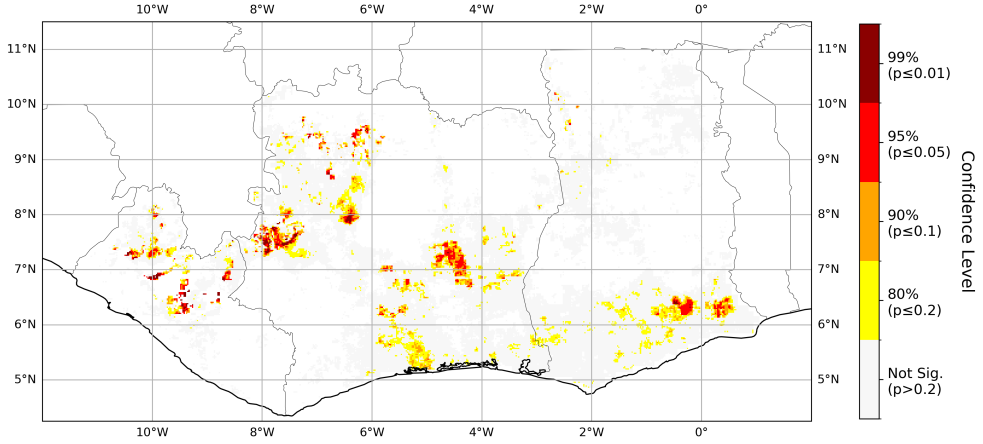

(b) Negatively correlated areas

Figure C.26: Statistical significance levels (80%, 90%, 95%, 99%, and not significant) for the Pearson's r correlation between full Harmattan dust (November–March) and full rainfall (April–September) across Liberia, Côte d'Ivoire, and Ghana, for areas with (a) positive and (b) negative correlations.

Figure C.27 shows the distribution of pixels with the confidence level above 90% correlations between the full Harmattan (November-March) and full rainfall (April-September) across the years. The full Harmattan period (November–March) spans two calendar years; the year label refers to the starting November (e.g., 2018 represents November 2018 to March 2019). Only the years up to 2023 is shown because the rainfall 2025 July-September has not occurred yet. The variance of positively correlated pixels was signif-

icantly lower compared to the negatively correlated pixels. The correlation of positively correlated pixels was much higher than that of negatively correlated pixels as well.

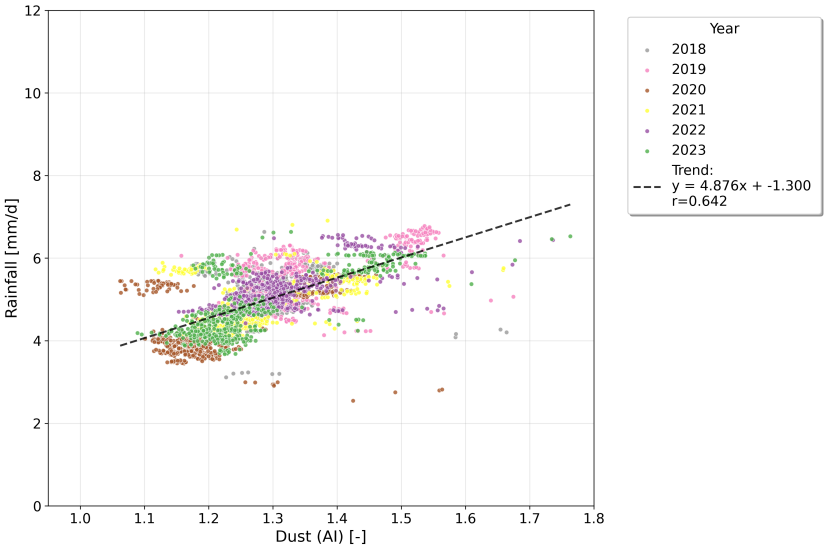

(a) Pixels with above 90% confidence level positive correlations. The dashed black line indicates the linear regression trend (y = 4.876x − 1.300), with a Pearson's correlation coefficient of $r = 0.642$.

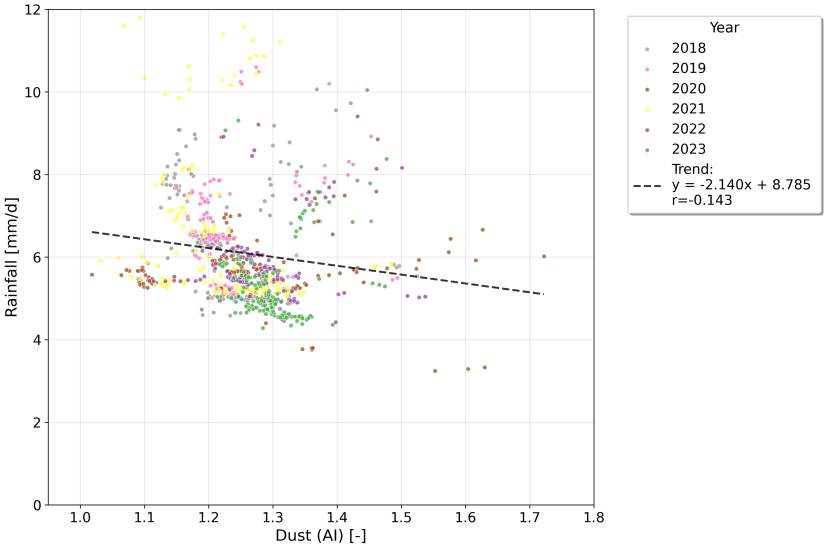

(b) Pixels with above 90% confidence level negative correlations. The dashed black line indicates the linear regression trend (y = -2.140x + 8.785), with a Pearson's correlation coefficient of $r = -0.143$.

Figure C.27: Relationship between November–March mean dust, represented by Aerosol Index (AI), and April–September mean rainfall for pixels with (a) statistically significant positive correlations ($p < 0.10$) and (b) statistically significant negative correlations ($p < 0.10$) across all years (2018–2023(up to September 2024 rainfall)). Each point represents a spatially averaged value for a given year, color-coded by year.

Appendix C.2. Full Harmattan to Early rainfall

Figure C.28 shows the correlation between full Harmattan (November-March) and early rainfall (April-May). The overall correlation was weaker compared to other seasonal pairs. Positive correlations were observed in the central to east regions of Côte d'Ivoire. Negative correlations were observed at the northwestern regions of Côte d'Ivoire, and southern Ghana also exhibited a weak negative correlation. Negative correlations were also found weakly in northern Liberia and some parts of northern Ghana. Figure C.29 shows the statistical significance of the calculated correlations. High statistical significance is observed only in northern regions of Côte d'Ivoire above 8 °N.

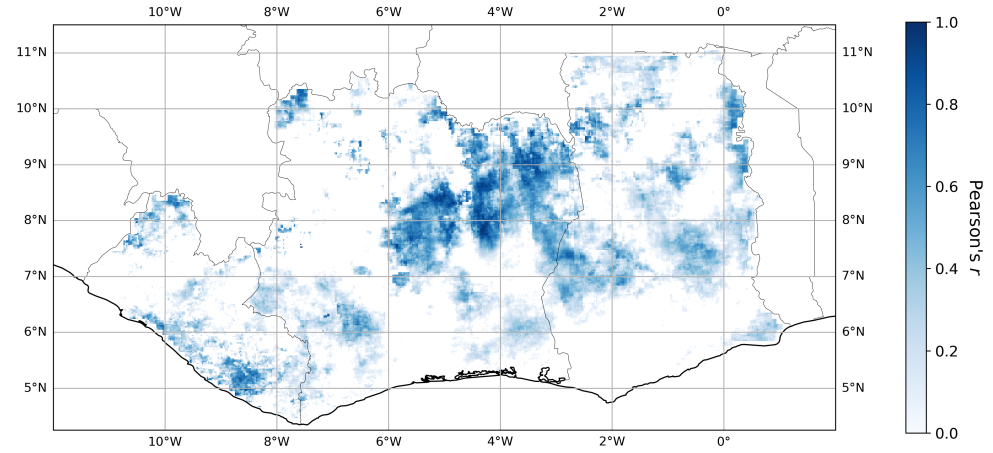

(a) Positive correlation

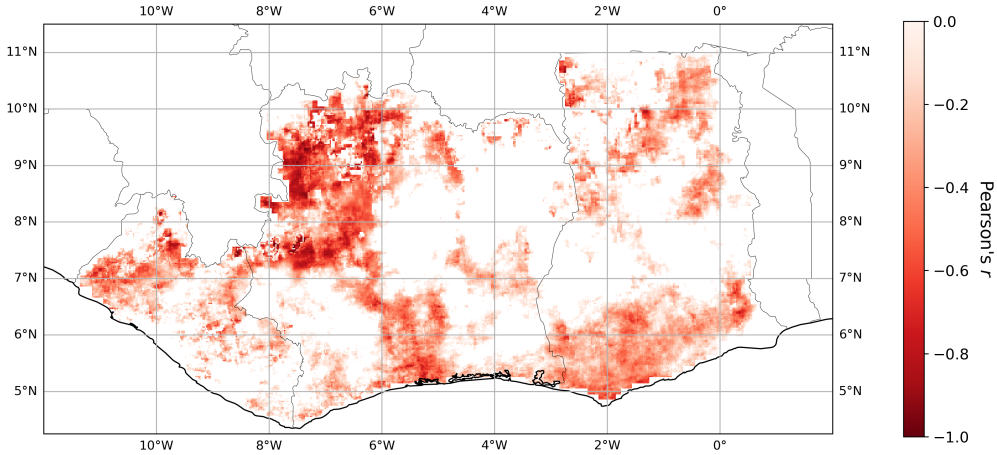

(b) Negative correlation

Figure C.28: Calculated Pearson's r correlation coefficients across Liberia, Côte d'Ivoire and Ghana for full Harmattan dust (November-March) and early rainfall (April-May) for (a) positive correlation and (b) negative correlation.

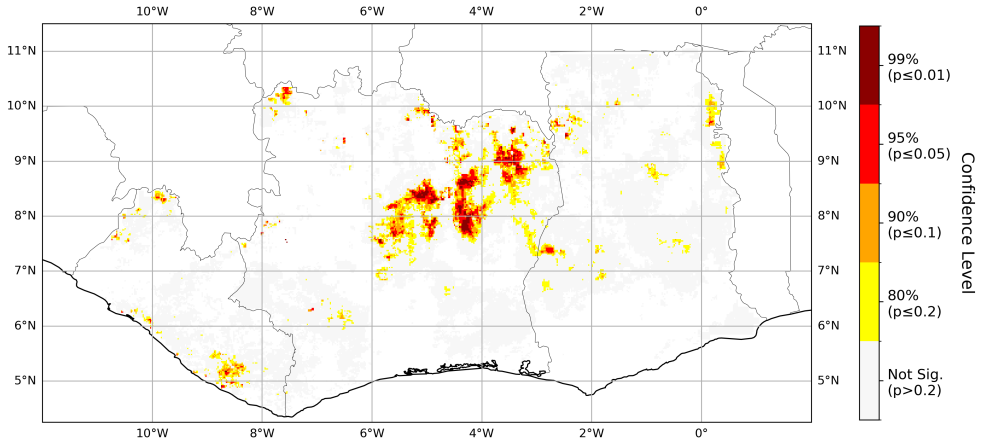

(a) Positively correlated areas

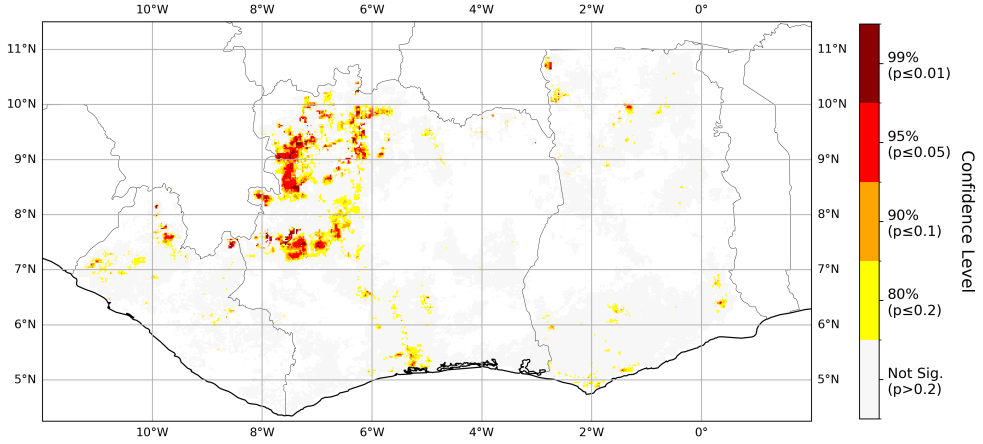

(b) Negatively correlated areas

Figure C.29: Statistical significance levels (80%, 90%, 95%, 99%, and not significant) for the Pearson's r correlation between full Harmattan dust (November–March) and early rainfall (April–May) across Liberia, Côte d'Ivoire, and Ghana, for areas with (a) positive and (b) negative correlations.

Figure C.30 shows the distribution of pixels with the confidence level above 90% correlations between the full Harmattan (November-March) and early rainfall (April-May) across the years. For positively correlated pixels, the distribution indicated a high correlation of r = 0.711. The values were clustered around the AI values between 1.1 and 1.4 [-], correspondingly, rainfall of 1.8 to 6 [mm/d]. For negatively correlated pixels, the distribution indicated a moderate correlation of r = -0.504. The negatively correlated

pixels indicated a wider spread approximately from 1 to 1.7 [-] compared to the positively correlated pixels.

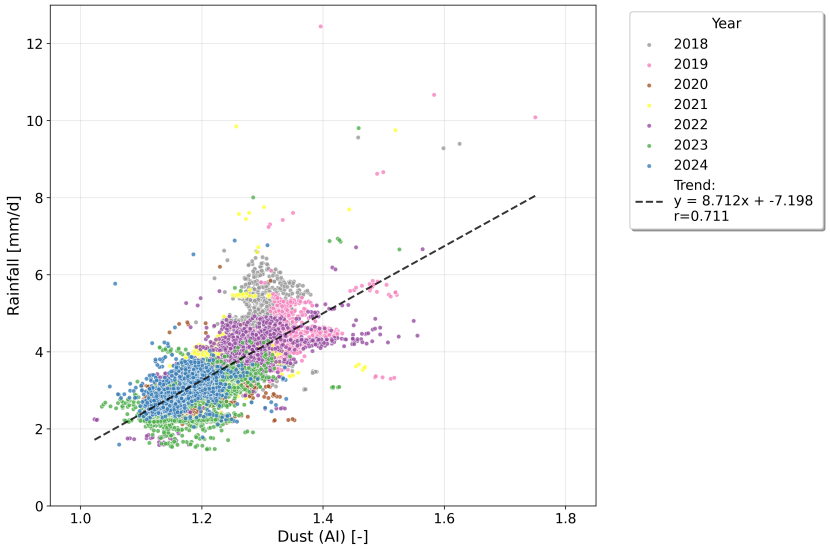

(a) Pixels with above 90% confidence level positive correlations. The dashed black line indicates the linear regression trend (y = 8.712x − 7.198), with a Pearson's correlation coefficient of $r = 0.711$.

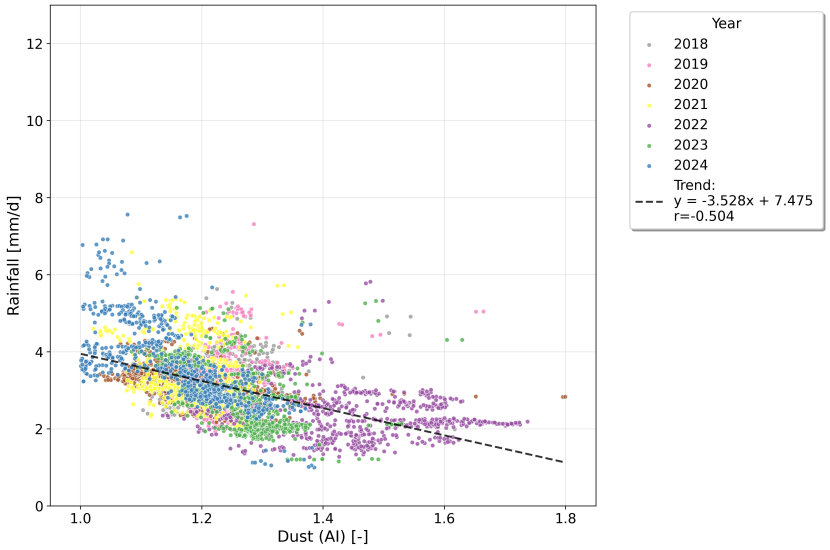

(b) Pixels with above 90% confidence level negative correlations. The dashed black line indicates the linear regression trend (y = -3.528x + 7.475), with a Pearson's correlation coefficient of $r = -0.504$.

Figure C.30: Relationship between November–March mean dust, represented by Aerosol Index (AI), and April–May mean rainfall for pixels with (a) statistically significant positive correlations ($p < 0.10$) and (b) statistically significant negative correlations ($p < 0.10$) across all years (2018–2024 (up to May 2025 rainfall)). Each point represents a spatially averaged value for a given year, color-coded by year.

Appendix C.3. Late Harmattan to Full rainfall

Figure C.31 shows the correlation between late Harmattan (February-March) and full rainfall (April-September). The northern and southern regions of the study area exhibited positive correlations. The central regions between 7°N and 9 °N exhibited negative correlations. Figure C.32 shows the statistical significance of the calculated correlations. Some regions in northern and central Côte d'Ivoire, and southern Liberia exhibited high statistical significance.

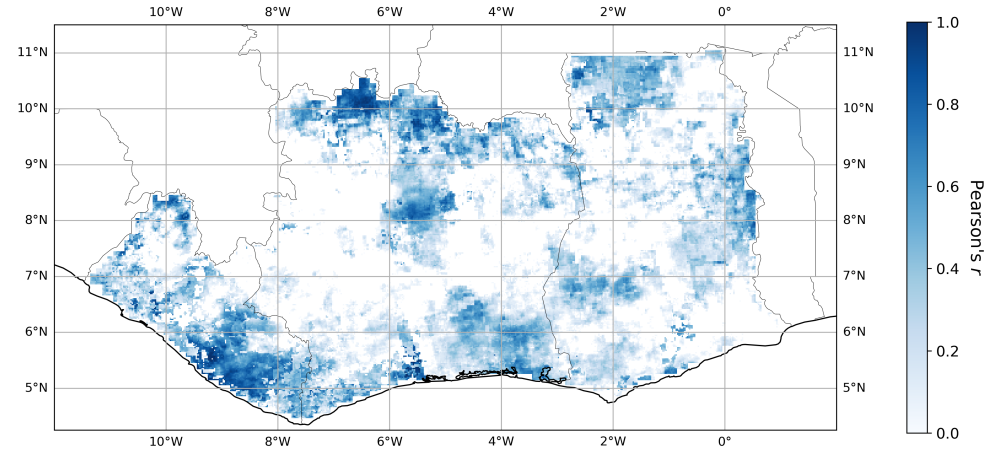

(a) Positive correlation

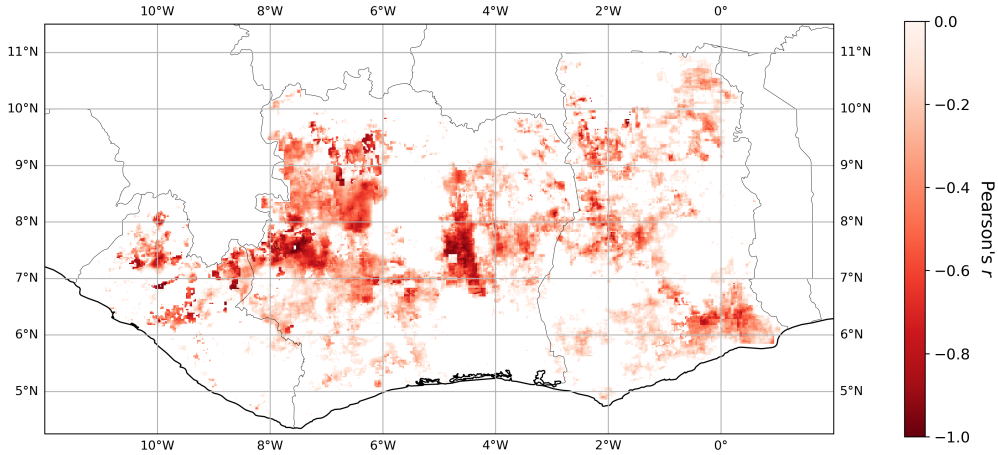

(b) Negative correlation

Figure C.31: Calculated Pearson's r correlation coefficients across Liberia, Côte d'Ivoire and Ghana for late Harmattan dust (February-March) and full rainfall (April-September) for (a) positive correlation and (b) negative correlation.

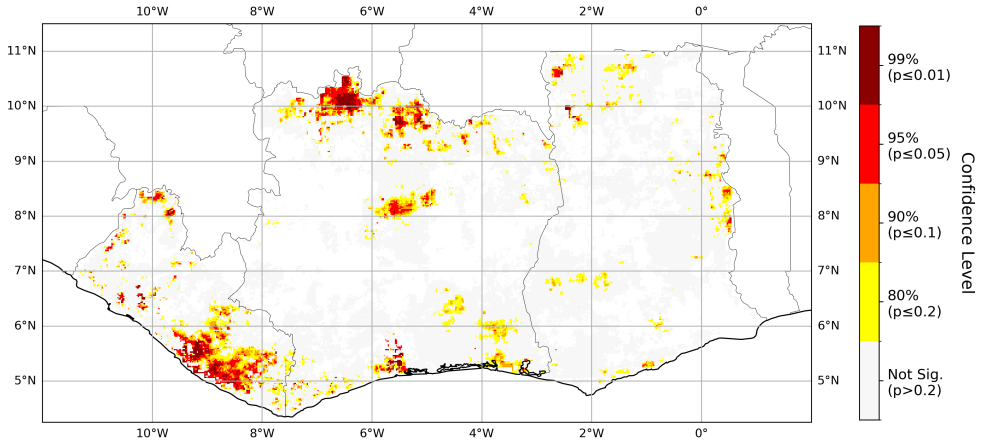

(a) Positively correlated areas

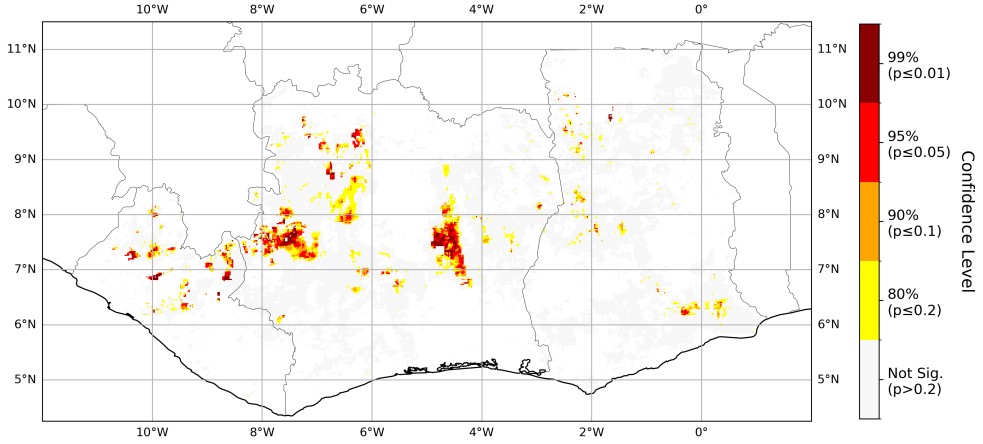

(b) Negatively correlated areas

Figure C.32: Statistical significance levels (80%, 90%, 95%, 99%, and not significant) for the Pearson's r correlation between late Harmattan dust (February–March) and full rainfall (April–September) across Liberia, Côte d'Ivoire, and Ghana, for areas with (a) positive and (b) negative correlations.

Figure C.33 shows the distribution of pixels with the confidence level above 90% correlations between the late Harmattan (February-March) and full rainfall (April-September) across the years. For positively correlated pixels, the distribution indicate the correlation was moderately weak with $r = 0.393$. Also, the spread of rainfall range was tight, most pixels falling between 2 to 6 mm/d. For negatively correlated pixels, the correlation of the distribution was also moderately weak, with r = -0.406. More outliers were

observed for the negatively correlated pixels.

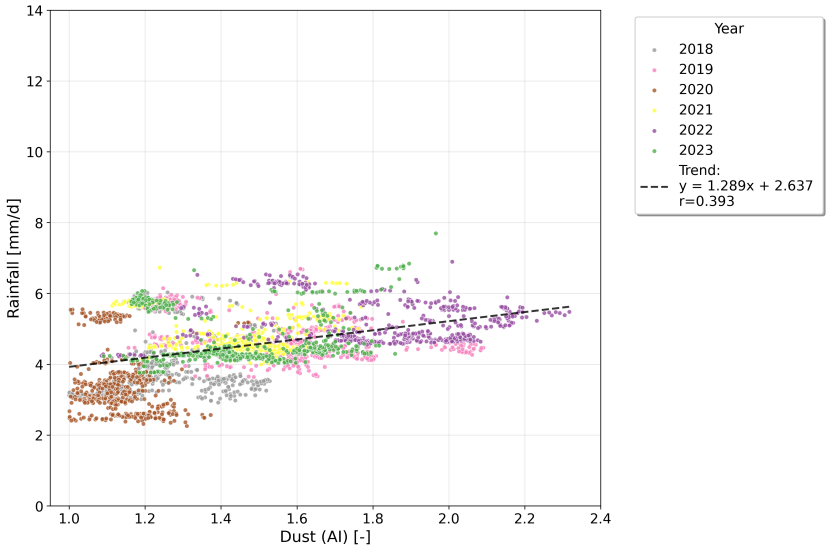

(a) Pixels with above 90% confidence level positive correlations. The dashed black line indicates the linear regression trend (y = 1.289x − 2.637), with a Pearson's correlation coefficient of $r = 0.393$.

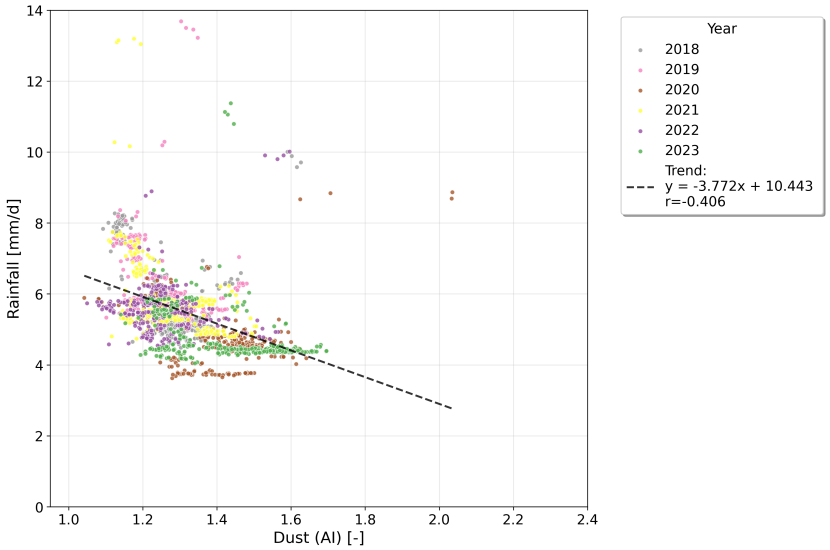

(b) Pixels with above 90% confidence level negative correlations. The dashed black line indicates the linear regression trend (y = -3.772x + 10.443), with a Pearson's correlation coefficient of $r = -0.406$.

Figure C.33: Relationship between February–March mean dust, represented by Aerosol Index (AI), and April–September mean rainfall for pixels with (a) statistically significant positive correlations ($p < 0.10$) and (b) statistically significant negative correlations ($p < 0.10$) across all years (2019–2023 (up to September 2024 rainfall)). Each point represents a spatially averaged value for a given year, color-coded by year.

Appendix D. Examples of variations of late Harmattan dust and early rainfall relations over the years for the most strongly correlated pixels

Figure D.34 shows the changes in the relation between late Harmattan dust (February-March) and early rainfall (April-May) for the pixels that indicated the strongest correlations as examples. The strongest correlations were found at 7.72 °N, 4.41 °W for the positive correlation of $r = 0.95$ and at 9.31 °N, 7.37 °W for the negative correlation of r = -0.98.

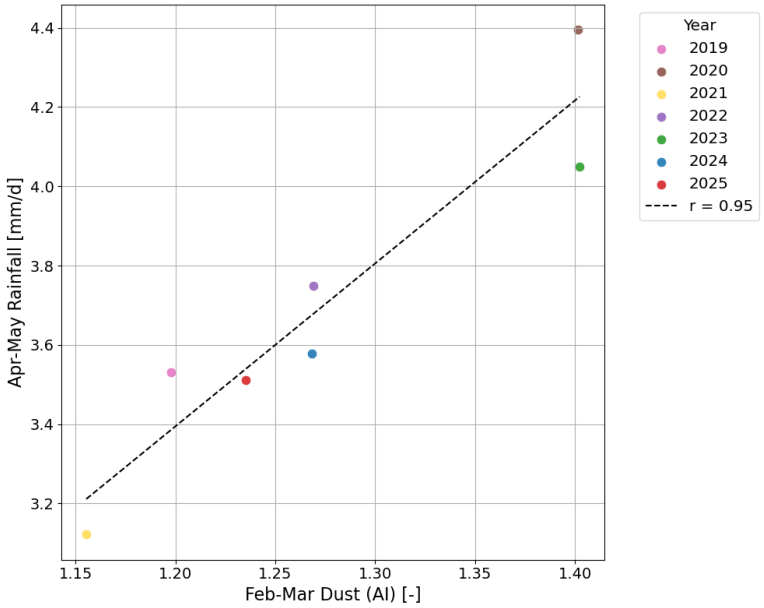

(a)

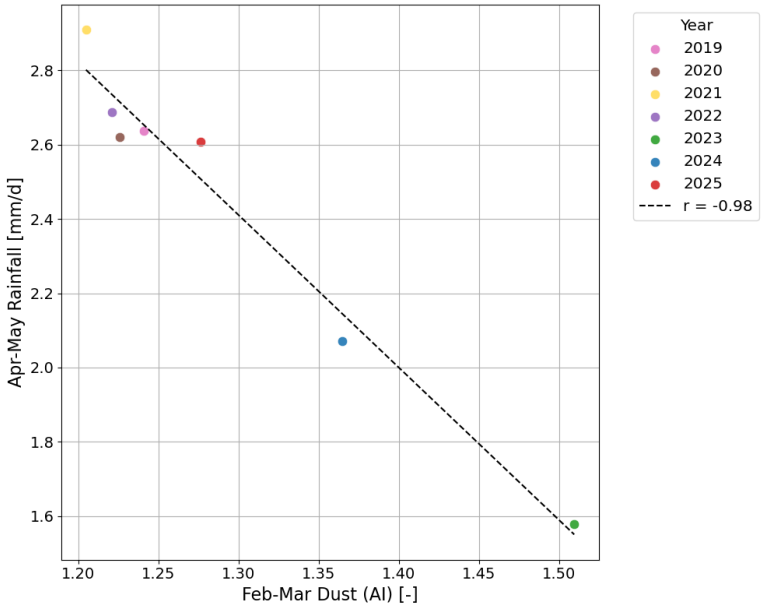

(b)

Figure D.34: Examples of yearly variations in late Harmattan (February-March) dust and early rainfall (April-May) for the most strongly correlated pixels. (a) for the positively correlated pixel at 7.72 °N, 4.41 °W. (b) for the negatively correlated pixel at 9.31 °N, 7.37 °W.

Appendix E. Spatial distribution of (February-March) dust and (April-May) rainfall

Figure E.35 shows the spatial distribution the mean dust in February-March and April-May, and mean rainfall in April-May across the study area from 2019 to 2025. The years with a high dust load in February-March generally exhibited a lower dust load in April-May, especially in coastal areas. Correspondingly, the areas affected by this relation exhibited higher early rainfall in April-May. The rainfall data for 2025 is based on IMERG Late data, whereas data for other years comes from IMERG Final data. As a result, the 2025 data may have greater uncertainties compared to other years.

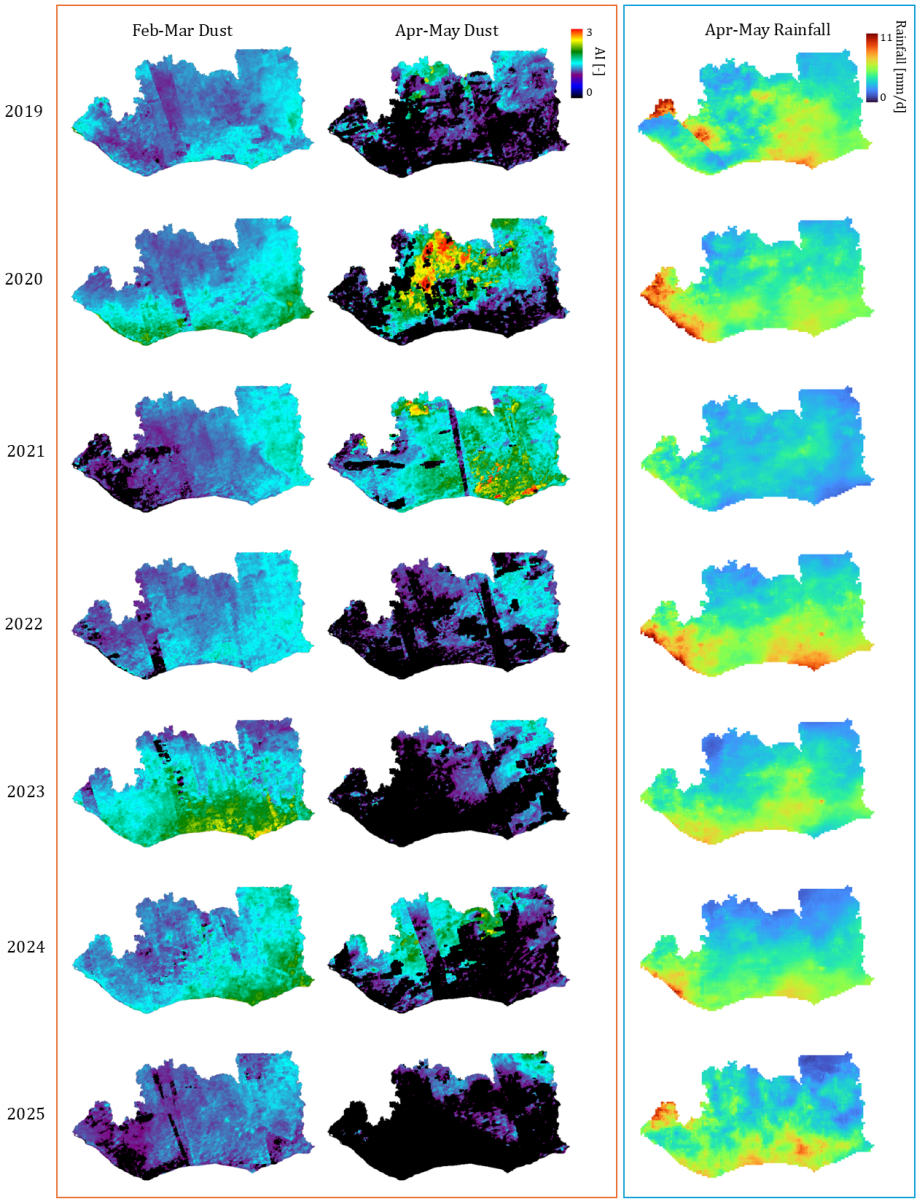

Figure E.35: Spatial distribution of the mean dust, represented by Aerosol Index (AI), for February–March and April–May, and mean rainfall for April–May over the study area for investigated years 2019-2025.

Appendix E.1. Granger Causality Test

Granger causality test examines whether a time series can predict another, although this is not a true causation (Granger, 1969). This statistical test has been widely applied in different disciplines and recent applications include detecting climate teleconnections in climate science (Silva et al., 2021).

This test was conducted to see the predictability of rainfall using Harmattan dust, which evaluates whether past values of one time series improve the prediction of another.

For the test, two regressions are performed:

1. **Restricted model** (rainfall predicted only from its own past values):

$$Y_t = \alpha_0 + \sum_{i=1}^{p} \alpha_i Y_{t-i} + \varepsilon_t$$

2. **Unrestricted model** (rainfall predicted from both its own and dust's past values):

$$Y_t = \beta_0 + \sum_{i=1}^{p} \beta_i Y_{t-i} + \sum_{j=1}^{p} \gamma_j X_{t-j} + \eta_t$$

In this study, $Y(t)$: Rainfall and $X(t)$: Harmattan dust (UVAI mean values)

The Granger causality test compares the residual sum of squares (SSR) from the restricted and unrestricted models using the F-statistic:

$$F = \frac{(\mathrm{SSR}_{\mathrm{restricted}} - \mathrm{SSR}_{\mathrm{unrestricted}})}{\mathrm{SSR}_{\mathrm{unrestricted}}/(n-k)}$$

where $\mathrm{SSR}_{\mathrm{restricted}}$: Sum of squared residuals from the restricted model, $\mathrm{SSR}_{\mathrm{unrestricted}}$: Sum of squared residuals from the unrestricted model, n: Number of observations, and k: Number of parameters in the unrestricted model

The resulting F-statistic is used to compute the p-value. If the p-value is below a certain significance level, the null hypothesis is rejected, and conclude that X Granger-causes Y (Shojaie and Fox, 2022).

Appendix E.1.1. Results

Figure E.36 shows the results of the Granger causality test for the relations between late Harmattan and early rainfall, highlighting areas with statistically significant relationships. In parts of the southwestern coastal region, especially along the coast in Côte d'Ivoire and along the border between Côte d'Ivoire and Liberia, high statistical significance is observed. These location showed strong positive correlations between late Harmattan dust and early rainfall. This means that the additional information provided by dust data improves the prediction of rainfall, compared to using only the past rainfall data for prediction. This suggests that early precipitation can potentially be predicted from dust in the late Harmattan. Northwestern to central Ghana and northwestern Côte d'Ivoire, where negative correlations between late Harmattan and early rainfall was observed, also indicate statistical significance from the Granger causality test in some parts, but not for all regions. Nevertheless, the spatial patterns of statistically significant Granger causality do not fully correspond to those of high correlated areas observed in Figure 3. Some locations without strong correlations still exhibit statistically significant Granger causality, such as the southeastern regions of Ghana. Overall, statistically significant locations are scattered throughout the study area, but majority of the areas did not show significance.

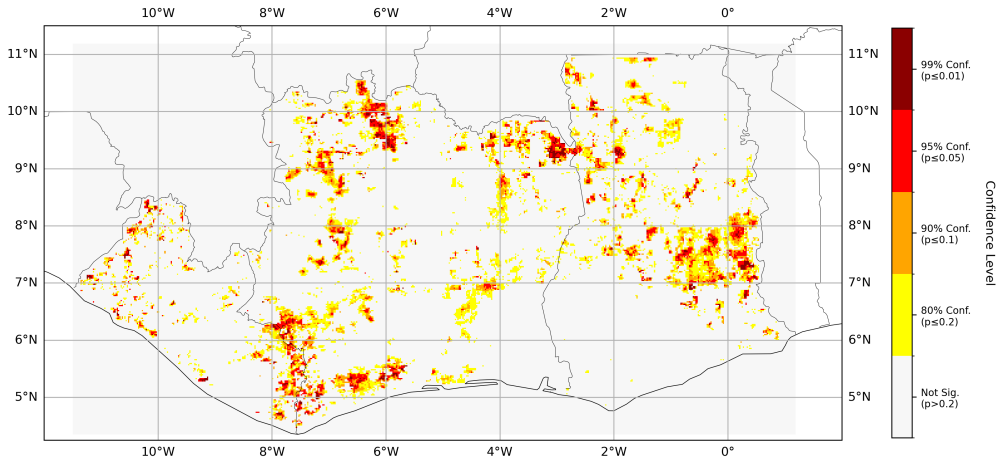

Figure E.36: Granger Causality Test statistical significance across Liberia, Côte d'Ivoire and Ghana for late Harmattan dust (February-March) and early rainfall (April-May) at different confidence levels of 80, 90, 95, 99%

References

Abu, I.O., Szantoi, Z., Brink, A., Robuchon, M., Thiel, M., 2021. Detecting cocoa plantations in côte d'ivoire and ghana and their implications on protected areas. Ecological indicators 129, 107863.

Adet, L., Rozendaal, D.M., Zuidema, P.A., Vaast, P., Anten, N.P., 2024. Cocoa tree performance and yield are affected by seasonal rainfall reduction. Agricultural Water Management 302, 108995.

Adetunji, J., Ong, C., 1989. The concentration of trace elements in the harmattan haze. Discovery and Innovations 1, 63–66.

Andreae, M.O., 2019. Emission of trace gases and aerosols from biomass burning–an updated assessment. Atmospheric Chemistry and Physics 19, 8523–8546.

Anuforom, A., Akeh, L., Okeke, P., Opara, F., 2007. Inter-annual variability and long-term trend of uv-absorbing aerosols during harmattan season in sub-saharan west africa. Atmospheric Environment 41, 1550–1559.

Apituley, A., Pedergnana, M., Sneep, M., Veefkind, J.P., Loyola, D., Landgraf, J., Borsdorff, T., 2024. Sentinel-5 precursor/TROPOMI Level 2 Product User ManualCarbon Monoxide. Technical Report. Royal Netherlands Meteorological Institute, Ministry of Infrastructure and Water Management.

Asitoakor, B.K., Asare, R., Ræbild, A., Ravn, H.P., Eziah, V.Y., Owusu, K., Mensah, E.O., Vaast, P., 2022. Influences of climate variability on cocoa health and productivity in agroforestry systems in ghana. Agricultural and Forest Meteorology 327, 109199.

Aweda, F., Falaiye, O., Samson, T., 2023. Heavy metal concentration in harmattan dust across selected stations in nigeria. Jordan Journal of Physics 16, 413–422.

Balarabe, M., 2019. The thirty years trend analysis of harmattan season visibility and temperature in sahel zone of nigeria. Physics Memoir-Journal of Theoretical & Applied Physics 1, 15–21.

Balarabe, M., Abdullah, K., Nawawi, M., Khalil, A.E., et al., 2016. Monthly temporal-spatial variability and estimation of absorbing aerosol index using ground-based meteorological data in nigeria. Atmospheric and Climate Sciences 6, 425.

Balarabe, M., Tan, F., Abdullah, K., Nawawi, M.M., 2015. Temporal-spatial variability of seasonal aerosol index and visibility—a case study of nigeria, in: 2015 International Conference on Space Science and Communication (IconSpace), IEEE. pp. 459–464.

Berthou, S., Rowell, D.P., Kendon, E.J., Roberts, M.J., Stratton, R.A., Crook, J.A., Wilcox, C., 2019. Improved climatological precipitation characteristics over west africa at convection-permitting scales. Climate Dynamics 53, 1991–2011.

Borsdorff, T., Campos, T., Kille, N., Volkamer, R., Landgraf, J., 2022. Vertical information of co from tropomi total column measurements in context of the cams-ifs data assimilation scheme. Atmospheric Measurement Techniques Discussions 2022, 1–20.

Brunner, C., Brem, B.T., Collaud Coen, M., Conen, F., Hervo, M., Henne, S., Steinbacher, M., Gysel-Beer, M., Kanji, Z.A., 2021. The contribution of saharan dust to the ice-nucleating particle concentrations at the high altitude station jungfraujoch (3580 m asl), switzerland. Atmospheric Chemistry and Physics 21, 18029–18053.

Chiemeka, I., Chineke, T., 2009. Evaluating the global solar energy potential at uturu, nigeria. International Journal of Physical Sciences 4, 115–119.

Climate Central, 2025. Climate change is heating up West Africa's cocoa belt. Technical Report. Climate Central.

Delgado-Ospina, J., Molina-Hernandez, J.B., Chaves-Lopez, C., Romanazzi, G., Paparella, A., 2021. The role of fungi in the cocoa production chain and the challenge of climate change. Journal of Fungi 7, 202.

Energy & Climate, 2025. Climate impacts on cocoa. Technical Report. Energy & Climate.

European Space Agency, . Copernicus sentinel-5p mapping portal. URL: `https://maps.s5p-pal.com/aai/`. accessed: 2025-06-04.

Fink, A.H., Engel, T., Ermert, V., Van Der Linden, R., Schneidewind, M., Redl, R., Afiesimama, E., Thiaw, W.M., Yorke, C., Evans, M., et al., 2017. Mean climate and seasonal cycle. Meteorology of tropical West Africa: The forecasters' handbook , 1–39.

Giles, D.M., Sinyuk, A., Sorokin, M.G., Schafer, J.S., Smirnov, A., Slutsker, I., Eck, T.F., Holben, B.N., Lewis, J.R., Campbell, J.R., et al., 2019. Advancements in the aerosol robotic network (aeronet) version 3 database–automated near-real-time quality control algorithm with improved cloud screening for sun photometer aerosol optical depth (aod) measurements. Atmospheric Measurement Techniques 12, 169–209.

Gong, C., Eltahir, E., 1996. Sources of moisture for rainfall in west africa. Water Resources Research 32, 3115–3121.

de Graaf, M., 2024. TROPOMI ATBD of the Aerosol Optical Thickness. Technical Report. Royal Netherlands Meteorological Institute, Ministry of Infrastructure and Water Management.

Granger, C.W., 1969. Investigating causal relations by econometric models and cross-spectral methods. Econometrica: journal of the Econometric Society , 424–438.

Guehaz, R., Sivakumar, V., Mbatha, N., 2024. A case study on the dust storm that occurred on march 13–18, 2022, over the algerian sahara, using satellite remote sensing. Journal of Atmospheric and Solar-Terrestrial Physics 264, 106345.

Hamilton, R., Archbold, J., Douglas, C., 1945. Meteorology of nigeria and adjacent territory. Quarterly Journal of the Royal Meteorological Society 71, 231–264.

Hayward, D.F., Oguntoyinbo, J., 2019. Climatology of West Africa. Routledge.

Herman, J., Bhartia, P., Torres, O., Hsu, C., Seftor, C., Celarier, E., 1997. Global distribution of uv-absorbing aerosols from nimbus 7/toms data. Journal of Geophysical Research: Atmospheres 102, 16911–16922.

Huffman, G.J., Bolvin, D.T., Joyce, R., Nelkin, E.J., Tan, J., Braithwaite, D., Hsu, K., Kelley, O.A., Nguyen, P., Sorooshian, S., Watters, D.C., West,

B.J., Xie, P., 2023. Algorithm Theoretical Basis Document (ATBD) NASA Global Precipitation Measurement (GPM) Integrated Multi-satellitE Retrievals for GPM (IMERG) Version 07. Technical Report. National Aeronautics and Space Administration.

International Cocoa Organization, . Growing cocoa. URL: https://www.icco.org/growing-cocoa/#:~:text=Variations%20in%20the%20yield%20of,should%20not%20exceed%20three%20months. accessed: 2025-06-04.

International Cocoa Organization, 2025. Data on production and grindings of cocoa beans. https://www.icco.org/wp-content/uploads/Production_QBCS-LI-No.-1.pdf. Accessed: 2025-06-02.

Kabo-bah, A.T., Amo-Boateng, M., Kabo-bah, K., Sey, N.E.N., Siabi, E., Okyereh, S., Sarquah, K., 2019. Sendai framework implementation–a regional assessment of wildfires in west africa .

Läderach, P., Martinez-Valle, A., Schroth, G., Castro, N., 2013. Predicting the future climatic suitability for cocoa farming of the world's leading producer countries, ghana and côte d'ivoire. Climatic change 119, 841–854.

Lyngsie, G., Awadzi, T., Breuning-Madsen, H., 2011. Origin of harmattan dust settled in northern ghana—long transported or local dust? Geoderma 167, 351–359.

Mao, Q., Huang, C., Chen, Q., Zhang, H., Yuan, Y., 2019. Satellite-based identification of aerosol particle species using a 2d-space aerosol classification model. Atmospheric Environment 219, 117057.

McTainsh, G., 1980. Harmattan dust deposition in northern nigeria. Nature 286, 587–588.

Mensah, E.O., Ræbild, A., Asare, R., Amoatey, C.A., Markussen, B., Owusu, K., Asitoakor, B.K., Vaast, P., 2023. Combined effects of shade and drought on physiology, growth, and yield of mature cocoa trees. Science of the Total Environment 899, 165657.

National Aeronautics and Space Administration, . Aerosol optical depth. URL: https://earthobservatory.nasa.gov/global-maps/MODAL2_M_AER_OD. accessed: 2025-06-06.

NATIONAL CENTERS FOR ENVIRONMENTAL INFORMATION, 2020. Global summary of the day. URL: https://www.ncei.noaa.gov/data/global-summary-of-the-day/doc/readme.txt. accessed: 2025-06-06.

Obilor, E.I., Amadi, E.C., 2018. Test for significance of pearson's correlation coefficient. International Journal of Innovative Mathematics, Statistics & Energy Policies 6, 11–23.

Oluleye, A., Jimoh, O., 2018. Influence of atmospheric circulation patterns on dust transport during harmattan period in west africa. Pollution 4, 9–27.

Rosenfeld, D., Nirel, R., 1996. Seeding effectiveness the interaction of desert dust and the southern margins of rain cloud systems in israel. Journal of Applied Meteorology and Climatology 35, 1502–1510.

Rosenfeld, D., Rudich, Y., Lahav, R., 2001. Desert dust suppressing precipitation: A possible desertification feedback loop. Proceedings of the National Academy of Sciences 98, 5975–5980.

Schepanski, K., Heinold, B., Tegen, I., 2017. Harmattan, saharan heat low, and west african monsoon circulation: modulations on the saharan dust outflow towards the north atlantic. Atmospheric Chemistry and Physics 17, 10223–10243.

Schroth, G., Läderach, P., Martínez-Valle, A.I., Bunn, C., 2015. Climate vulnerability and adaptation of the smallholder cocoa and coffee value chains in Liberia. Technical Report. Working Paper.

Schroth, G., Läderach, P., Martinez-Valle, A.I., Bunn, C., Jassogne, L., 2016. Vulnerability to climate change of cocoa in west africa: Patterns, opportunities and limits to adaptation. Science of the Total Environment 556, 231–241.

Schwanghart, W., Schütt, B., 2008. Meteorological causes of harmattan dust in west africa. Geomorphology 95, 412–428.

Shojaie, A., Fox, E.B., 2022. Granger causality: A review and recent advances. Annual Review of Statistics and Its Application 9, 289–319.

Silva, F.N., Vega-Oliveros, D.A., Yan, X., Flammini, A., Menczer, F., Radicchi, F., Kravitz, B., Fortunato, S., 2021. Detecting climate teleconnections with granger causality. Geophysical Research Letters 48, e2021GL094707.

Stein Zweers, D., 2022. TROPOMI ATBD of the UV aerosol index. Technical Report. Royal Netherlands Meteorological Institute, Ministry of Infrastructure and the environment.

Sunnu, A., Afeti, G., Resch, F., 2008. A long-term experimental study of the saharan dust presence in west africa. Atmospheric Research 87, 13–26.

Taylor, J., Beillard, M.J., Galloway, J.D., 2025. Ghana - Cocoa Sector Overview - 2025. Technical Report. United States Department of Agriculture, Foreign Agricultural Service.

Tegen, I., Schepanski, K., Heinold, B., 2013. Comparing two years of saharan dust source activation obtained by regional modelling and satellite observations. Atmospheric Chemistry and Physics 13, 2381–2390.

Torres, O., Jethva, H., Ahn, C., Jaross, G., Loyola, D.G., 2020. Tropomi aerosol products: Evaluation and observations of synoptic scale carbonaceous aerosol plumes during 2018–2020. Atmospheric measurement techniques discussions 2020, 1–20.

Torres, O., Tanskanen, A., Veihelmann, B., Ahn, C., Braak, R., Bhartia, P.K., Veefkind, P., Levelt, P., 2007. Aerosols and surface uv products from ozone monitoring instrument observations: An overview. Journal of Geophysical Research: Atmospheres 112.

Twohy, C.H., Kreidenweis, S.M., Eidhammer, T., Browell, E.V., Heymsfield, A.J., Bansemer, A.R., Anderson, B.E., Chen, G., Ismail, S., DeMott, P.J., et al., 2009. Saharan dust particles nucleate droplets in eastern atlantic clouds. Geophysical Research Letters 36.

Veefkind, J.P., Aben, I., McMullan, K., Förster, H., De Vries, J., Otter, G., Claas, J., Eskes, H., De Haan, J., Kleipool, Q., et al., 2012. Tropomi on the esa sentinel-5 precursor: A gmes mission for global observations

of the atmospheric composition for climate, air quality and ozone layer applications. Remote sensing of environment 120, 70–83.

World Bank, 2025. Climate change knowledge portal. URL: https://climateknowledgeportal.worldbank.org/. accessed: 2025-06-04.

Wu, H., Taylor, J.W., Langridge, J.M., Yu, C., Allan, J.D., Szpek, K., Cotterell, M.I., Williams, P.I., Flynn, M., Barker, P., et al., 2021. Rapid transformation of ambient absorbing aerosols from west african biomass burning. Atmospheric Chemistry and Physics 21, 9417–9440.

Yao, I., Beillard, M.J., Galloway, J.D., Taylor, J., 2025. Cote d'Ivoire - Cocoa Sector Overview - 2025. Technical Report. United States Department of Agriculture, Foreign Agricultural Service.

Yoroba, F., Kouassi, B.K., Diawara, A., Yapo, L.A., Kouadio, K., Tiemoko, D.T., Kouadio, Y.K., Koné, I.D., Assamoi, P., 2019. Evaluation of rainfall and temperature conditions for a perennial crop in tropical wetland: a case study of cocoa in côte d'ivoire. Advances in Meteorology 2019, 9405939.

Zhang, Y., Wang, N., Jin, S., 2025. Performance and evaluation of remote sensing satellites for monitoring dust weather in east asia. EGUsphere 2025, 1–32. URL: https://egusphere.copernicus.org/preprints/2025/egusphere-2025-992/, doi:10.5194/egusphere-2025-992.

Ștefănie, H.I., Radovici, A., Mereuță, A., Arghiuș, V., Cămărășan, H., Costin, D., Botezan, C., Gînscă, C., Ajtai, N., 2023. Variation of aerosol optical properties over cluj-napoca, romania, based on 10 years of aeronet data and modis maiac aod product. Remote Sensing 15, 3072.